Copyright © 1992, by the author(s).
All rights reserved.

Permission to make digital or hard copies of all or part of this work for personal or classroom use is granted without fee provided that copies are not made or distributed for profit or commercial advantage and that copies bear this notice and the full citation on the first page. To copy otherwise, to republish, to post on servers or to redistribute to lists, requires prior specific permission.

A THREE-DIMENSIONAL PHYSICALLY-BASED MODEL FOR LPCVD

by

Sherry Fen-hwei Lee

Memorandum No. UCB/ERL M92/69

22 May 1992

Memorandum No. UCB/ERL M92/69

22 May 1992

A THREE-DIMENSIONAL PHYSICALLY-BASED MODEL FOR LPCVD

by

Sherry Fen-hwei Lee

Memorandum No. UCB/ERL M92/69

22 May 1992

ELECTRONICS RESEARCH LABORATORY

College of Engineering
University of California, Berkeley
94720

Table of Contents

Chapter 1 Introduction 1
1.1 Background and Motivation 1
1.2 Thesis Organization 3

Chapter 2 Computational Fluid Dynamics 4
2.1 Introduction 4
2.2 Numerical Methods 4
2.3 Fundamental Properties 6
2.3.1 Conservation of Mass 6
2.3.2 Conservation of Momentum 7
2.3.3 Conservation of Energy 8
2.3.4 Conservation of Chemical Species 8
2.4 Computational Software 9
2.4.1 Fluent 9
2.4.2 PHOENICS 10

Chapter 3 LPCVD Furnace Model 15
3.1 Model Parameters 15
3.2 Furnace Description 16
3.3 Temperature Calculation 17
3.4 Longitudinal Flow 18
3.4.1 Reynold's Number 18
3.4.2 Prandtl and Peclet Numbers 19
3.5 Radial Flow 20
3.5.1 Multicomponent Diffusion 20
3.5.2 Thermal Diffusion 22

Chapter 4 Chemical Kinetics 24
4.1 One-Step Reaction 24
4.2 Two-Step Reaction 26
4.2.1 Volume Reaction 27
4.2.2 Surface Reaction 27
4.3 Phosphine-doped polysilicon 28

Chapter 5 Comparison with Actual Furnace 29
5.1 Introduction 29
5.2 Experiments 29
5.2.1 Heat Baffle Temperature 29
5.2.2 Wafer thickness and uniformity measurements 30
5.3 Simulated Undoped Polysilicon Deposition 31
5.3.1 Discretization of the Furnace Volume 31
5.3.2 Gas Velocities 34
5.3.3 Concentration and Depletion Effects 37

5.3.4 Deposition Rates 38
Chapter 6 Conclusions and Future Plans 42
Appendix A: Nomenclature 43
Appendix B: PHOENCS Q1 File 45
Appendix C: PHOENICS *Ground.f* File 50
References 53

List of Figures

Figure 1	Structure of the PHOENICS software	14
Figure 2	Deposition Furnace	16
Figure 3	Radial (y) and Longitudinal (z) Directions	18
Figure 4	Temperature Profile in Heat Baffle Region	30
Figure 5	Discretization of the Wafer Region	32
Figure 6	2D Grid with Heat Baffle and Wafers	33
Figure 7	3D Grid with Heat Baffle and PorousWafers	34
Figure 8	Inlet Velocity Vectors	35
Figure 9	Wafers: (a) No Reaction, (b) Surface Reaction	36
Figure 10	Within Wafer Non-uniformity	37
Figure 11	Silane Concentration Along the Tube	38
Figure 12	Silane Concentration Across Wafers	38
Figure 13	Simulated vs. Experimental Deposition Rates	39
Figure 14	Run 1- Simulated vs. Experimental Deposition Rates	40
Figure 15	Run 4- Simulated vs. Experimental Deposition Rates	40
Figure 16	Run 7- Simulated vs. Experimental Deposition Rates	41

Acknowledgment

I would like to express my deep appreciation and gratitude to my research advisor, Costas J. Spanos, for his generous support and guidance throughout my graduate studies. I also thank Dean Hodges for his continous support of the CAM program at Berkeley.

Many people helped with various aspects of this research, most notably Dr. K. Lin for his work in modelling LPCVD reactors and for conducting the experiments used in this thesis, Dr. J. Ignacio Ulacia F., Dr. Christoph Werner, and Christian Hopfmann for helping me model chemical reactions in the PHOENICS software package, and Henry Chang for aiding in the optimization process.

Special thanks are due to Eric Boskin for sharing his software expertise and for always providing insightful feedback. I also thank L. Massa-Lochridge for helping with the computer hardware aspects of the project. Thanks are also extended to the remaining members of the Berkeley CAM group, all of whom made my experiences at Berkeley a great pleasure: B. Bombay, R. Chen, Z. Daoud, M. Hosseini, S. Leang, H. Liu, J. Thomson, and E. Wen, and past members: Dr. N. Chang, H. Guo, Dr. K. Lin, T. Luan, and Dr. G. May.

I am grateful to Digital Equipment Corporation for sponsoring this work in the form of a fellowship since 1990. Prior to 1990, this research was jointly sponsored by National Science Foundation (Grant No. MIP 87-15557), Semiconductor Research Corporation, National Semiconductor, and Texas Instruments.

Chapter 1 Introduction

1.1 Background and Motivation

Today's VLSI technology is becoming increasingly complex, requiring sophisticated manufacturing facilities that are rising in cost. Over 70% of the cost of a new DRAM factory is spent on equipment, and predictions show that this trend will continue as the complexity of the processes increases [1]. With such complex processes, the equipment must meet strict performance standards, which leads to a growing need for meaningful equipment monitoring, diagnosis, and control. One process that is being pushed to its performance limits is chemical vapor deposition of thin films. For example, while older technologies could tolerate variations of ±5% across 100 *mm* wafers, new circuits require film thicknesses with variations less than ±2% across 150 *mm* wafers [2]. To achieve these goals, better equipment design and process control are necessary. Computer simulation can help both to reduce the equipment design cycle times and to optimize the process.

Many equipment models are created using statistical methods, such as factorial designs and regression analysis [3]. These methods, however, require a significant number of experiments, which consume a large amount of time and become quite expensive. Additionally, empirical models are usually valid only in a restricted range, and generally provide little or no physical insight. Thus, while empirical models are ideal for equipment that is being used in IC production, they are not suited for equipment design.

Physical modelling via computer simulation, on the other hand, can be used to model a variety of recipes and equipment designs, and can return results both quickly and cost effectively. For example, in the case of a new furnace design, the geometry can be changed numerous times in the simulator without having to build as many prototypes, thus

reducing the design cycle time. The effect of individual process parameters on the overall process can also be evaluated, thus aiding in the optimization of the process conditions.

Accurate simulation models depend on the proper formulations to represent the detailed processes. Therefore, physical models, based on the laws of fluid dynamics and chemical kinetics, require an accurate description of the boundary conditions and proper transport equations.

Several extensive studies on the physical modeling of undoped polysilicon low pressure chemical vapor deposition (LPCVD) have been published. Middleman and Yeckel [4] found that the dominant transport mechanism between the wafers in a tubular hot-wall system is diffusion, and that the flow in the annular region around the wafers does not significantly affect the deposition rate. Jensen *et al*'s [5,6] detailed mathematical model includes multicomponent transport effects. Roenigk and Jensen [6] improved upon the surface reaction rate equation developed by Classen et al [7]. A comprehensive study of the chemical species involved in the deposition process has been done by Coltrin *et al* [8], who developed a mathematical model which includes seventeen chemical species. Recently, Sachs [9] developed a one-dimensional finite difference model that uses a numerical optimizer on a series of statistically designed experiments to obtain the growth parameters. While the work discussed above rely on one-dimensional mathematical models to describe the process, Ulacia and Werner [10] have developed a three-dimensional model that uses a commercial numerical methods software package.

In this work, three-dimensional physical models of undoped polysilicon LPCVD are presented. The models can be used to optimize growth parameters such as gas flow, temperature, and pressure to achieve higher wafer uniformity across the furnace and across each wafer. Although current CPU performance limitations do not allow for real-time applications on the manufacturing floor, these models can be used to build a knowledge base for diagnosis and control.

1.2 Thesis Organization

An overview of computational fluid dynamics is provided in Chapter 2, along with a description of the software code used for the simulations. Chapter 3 explains the theory of fluid flow and details the fundamental properties included in the model. The chemical kinetics used in the model are described in Chapter 4, and simulation results compared to actual furnace runs are given in Chapter 5. Finally, in Chapter 6 the results are evaluated and further work is suggested.

Chapter 2 Computational Fluid Dynamics

2.1 Introduction

As the semiconductor manufacturing environment becomes dominated by more complex processes and equipment, in-depth understanding is necessary to implement state-of-the-art monitoring, diagnosis, and control. To this end, manufacturing engineers are developing sophisticated models to describe processes. A major area of interest involves fluid dynamics, which is important in processes such as deposition and plasma etching. Until the advent of high-speed computers, fluid flow analysis was performed by doing costly and time-consuming experiments. Presently, analysis can be augmented with computer simulations, which alleviate the need to perform extensive experiments. This simulation of fluid-flow, mass transfer, and heat transfer is the subject of Computational Fluid Dynamics (CFD).

CFD simulation is based on the equations describing the physical laws associated with transport phenomena. There are several benefits of physically-based simulation. Variables which are experimentally difficult to attain, such as species concentrations, can be calculated. A complete set of information may be obtained throughout the entire region, not only where the sensors are placed. In addition, the effect of each property can be examined, such as an increase in pressure or a ramped temperature.

2.2 Numerical Methods

To model a continuous, three-dimensional space via a set of equations, the space must be discretized into a finite number of cells. The grid is created over the entire physical space, with finer grid points in regions of high velocity, temperature, or concentration gradients. The unknown parameters can then be solved at each grid point. Most numerical

software packages use either the finite difference or the finite element method to discretise the space.

Due to the non-linearity and the size of the discretized system, an iterative solution must be used. At the start of a simulation, the variables at each grid point are given initial values. The variables are then updated, and are in turn used as the input for the next iteration. This continues until a convergent solution is found. The convergence criterion is usually met when the iterative solutions stabilize within limits set by the user.

Since several variables are introduced with each grid point, finer grids lead to longer simulation times. The furnace simulations require considerable computer time. For example, a two-dimensional simulation with 5292 grid points and 11 variables, not including chemical reactions, takes approximately 1.5 hours on an IBM RISC 6000 (520) to reach convergence (about 1000 iterations). If chemical reactions are modeled, the simulation takes about 2.4 hours for the same number of iterations. For a problem in three dimensions, which requires more grid points, simulation time can reach up to 10 hours. This is, however, still considerably less than the time needed to construct and experiment with a new reactor.

Table 1 tabulates some simulation times vs. number of variables solved, comparing two- and three-dimensional simulations. The first row shows the number of grid points and time for a three-dimensional simulation that models individual wafers, while the second row models the wafers as a "porous region," which is discussed in detail in Chapter 5. Basically, in the the porous region, there are fewer grid points between the wafers than if the wafers were modeled individually. Note that by not modelling individual wafers, significant computational time can be saved. The third and fourth rows are indicative of typical two-dimensional simulations with and without chemical reactions modeled, respectively.

Most simulations model steady-state behavior, although transient models are available. Transient models require solving the time derivatives of the equations, which results in much longer simulation times. The focus of this work is steady-state behavior.

dimensions	number of variables	number of cells	number of iterations	time (hours)
3	19	6,512	350	9.45
3	19	1,494	350	2.17
2	18	5,292	350	0.85
2	11	5,292	350	0.52

Table 1: Typical Simulation Times on an IBM RT 6000

2.3 Fundamental Properties

The four fundamental rules which are modeled in CFD codes are the conservation of mass, momentum, energy, and chemical species. The equations for conservation of mass and momentum together describe viscous flow of a pure isothermal fluid. Conservation of energy and of chemical species are necessary for non-isothermal fluids and for multicomponent mixtures.

2.3.1 Conservation of Mass

The equation for the conservation of mass, also known as the continuity equation, states that the rate of mass accumulation into a volume is equal to the net rate of mass efflux from that volume:

$$\underbrace{\frac{\partial \rho}{\partial t}}_{\text{rate of mass accumulation}} = - \underbrace{(\nabla \bullet \rho v)}_{\text{net rate of mass efflux}} \qquad (1)$$

where ρ is the density (*mass/unit volume*), and $\mathbf{v}$ is the velocity[1] (*time/unit length*). Equivalently, the equation describes the rate of change of density at a fixed point resulting from the changes in the mass velocity vector $\rho\mathbf{v}$. For steady-state flow, the rate of mass accumulation is zero. Thus, the continuity equation becomes

$$(\nabla \bullet \rho \mathbf{v}) = 0. \tag{2}$$

2.3.2 Conservation of Momentum

Conservation of momentum states that the sum of the forces acting on the control volume is equal to the rate of momentum accumulation within the volume plus the net rate of momentum efflux from that control volume. It is equivalent to Newton's second law of motion, $\mathbf{F} = m\mathbf{a}$:

$$\underbrace{\mathbf{F}}_{\text{sum of forces}} = \underbrace{\frac{\partial}{\partial t}\rho \mathbf{v}}_{\text{rate of momentum accumulation}} + \underbrace{\nabla \bullet \rho \mathbf{v}\mathbf{v}}_{\text{net rate efflux of momentum}} \tag{3}$$

The forces include those due to body forces such as gravity and to the normal stress and shear stress. This is expressed as:

$$\mathbf{F} = -\nabla p - \nabla \bullet \tau + \rho \mathbf{g} \tag{4}$$

where τ is the stress tensor, p is the pressure, and $\mathbf{g}$ is the gravitational force. Combining equations (3) and (4) results in the Navier-Stokes equation, which expresses Newton's second law of motion for a Newtonian fluid[2]:

---

1. Note that bold lower case characters denote column vectors. Please see Appendix A for a full list of the nomenclature used in this paper.

2. A Newtonian fluid is a fluid whose shear force per unit area is proportional to the negative of the local velocity gradient:

$$\tau_{yx} = -\mu \frac{dv_x}{dy}$$

where μ is the viscosity (*kg/m/sec*) and $\mathbf{v}$ is the velocity (*m/sec*).

$$\frac{\partial}{\partial t}\rho v + \nabla \bullet \rho v v = -\nabla p - \nabla \bullet \tau + \rho g \tag{5}$$

2.3.3 Conservation of Energy

The general form of the energy balance equation is:

$$\underbrace{\frac{\partial}{\partial t}\rho\left(\hat{U}+\frac{1}{2}|v|^2\right)}_{\text{rate of gain of energy per unit volume}} = -\underbrace{\left(\nabla \bullet \rho v\left(\hat{U}+\frac{1}{2}|v|^2\right)\right)}_{\text{rate of energy input per unit volume by convection}} - \underbrace{\nabla \bullet q}_{\text{rate of energy input per unit volume by conduction}} + \underbrace{\rho\,(v \bullet g)}_{\text{rate of work done per unit volume by gravity}}$$

$$- \underbrace{(\nabla \bullet p v)}_{\text{rate of work done per unit volume by pressure forces}} - \underbrace{(\nabla \bullet (\tau \bullet v))}_{\text{rate of work done per unit volume by viscous forces}} \tag{6}$$

where $\hat{U}$ is the internal energy per unit mass of fluid, $|v|$ is the magnitude of the local fluid velocity, and **q** is the heat flux vector. For the case of heat transfer of gases, the above equation can be rewritten, assuming ideal gases, constant thermal conductivity k, and neglecting viscous dissipation:

$$\rho C_v \frac{\partial T}{\partial t} = k\nabla^2 T - p(\nabla \bullet v) \tag{7}$$

where C_v is the heat capacity of the gas at constant volume per unit mass, and T is the temperature. For gases at constant pressure, this can be further modified to give:

$$\rho C_p \frac{\partial T}{\partial t} = k\nabla^2 T \tag{8}$$

where C_p is the constant-pressure specific heat.

2.3.4 Conservation of Chemical Species

When a chemical reaction is involved in the process, the chemical species must also balance. In the presence of a velocity field, the conservation equation states that the rate of

change of species concentration plus the inward diffusion flux of the species is equal to the net rate of species generation per unit volume.

$$\underbrace{\frac{\partial}{\partial t}(\rho w_i) + (\nabla \bullet \rho w_i v)}_{\text{rate of change of species concentration}} = -\underbrace{(\nabla \bullet j_i)}_{\text{inward flux}} + \underbrace{G_i}_{\text{production rate of species}} - \underbrace{R_i}_{\text{consumption rate of species}} \quad (9)$$

where w_i is the mass fraction, j_i is the mass flux relative to the mass average velocity, and G_i and R_i are the production and consumption rates of the ith species, respectively. The components of the mass flux include ordinary diffusion (Fick's first law), pressure diffusion, forced diffusion, and thermal diffusion. Obviously, ordinary diffusion is significant in the model because more than one species is involved, so that deposition depends on concentration gradients. Pressure diffusion, however, is only important if there is a pressure gradient imposed. In the case of LPCVD, which has a fairly uniform pressure, this is not a significant effect and therefore can be neglected. Forced diffusion can also be neglected, as this is of primary importance in ionic systems when there is a large electric field imposed. As mentioned in the next chapter, thermal gradients are small in the region where the wafers are processed, so thermal diffusion is also neglected.

2.4 Computational Software

2.4.1 Fluent

We began this project with the commercial software package Fluent (version 2.99 by Creare.x Inc.), which is a finite difference numerical methods solver [11]. Although the software easily solved radiative and flow problems via built-in functions, it was too restrictive for our purposes. Most notably, the code was not flexible enough to solve complex chemical equations. At the time of our use, Creare.x was in the process of updating

the code to include more relevant chemical kinetics. Since the updated code was unavailable, we decided to investigate other possible commercial CFD packages.

2.4.2 PHOENICS

The commercial CFD software PHOENICS was chosen for the project. PHOENICS employs the finite differencing scheme, and can provide conformal grids. PHOENICS consists of three main computer programs and three auxiliary programs, all written in FORTRAN. Given the proper boundary conditions and proper transport equations, it can be used to simulate fluid flow, heat transfer, and chemical kinetics. The main codes are the pre-processor Satellite, which interprets the problem description written in the PIL language, the processor Earth, which performs the necessary computations to solve the fluid flow equations, and the post-processor Photon, which graphically displays the output. Three auxiliary codes contain programs for grid manipulation and an on-line help facility [12, 13]. The function of each of the main codes is described in more detail below.

2.4.2.1 Satellite

As mentioned above, Satellite is the command interpreter. It receives its input from the user in the form of an input file, similar to that of the SPICE Circuit Simulator. The input file, called the Q1 file, contains commands which Satellite interprets. The language used in the Q1 file is the PHOENICS Input Language (PIL), which consists of abbreviated FORTRAN functions. The Q1 file used to represent our LPCVD model can be found in Appendix B.

The Q1 code contains three main sections. The first section defines the equipment parameters, such as reactor size and placement of the wafers. In addition, the grid is defined, and the variables to be stored or solved are specified. Solved variables are the parameters to be solved by the source code at each grid point, such as enthalpy, velocity, pressure, and concentration. In contrast, stored variables are those that can be computed

by the user given the solved variables. For example, the stored variable "temperature" can be calculated from the solved variable "enthalpy," and density can be in turn calculated from the temperature, pressure, and species concentration at each grid point. Deposition rates can also be computed from the concentration (see Appendix C for more details), so it too is a stored variable. Simple physical properties can be specified in the Satellite Q1 file, such as a constant density or temperature. If, however, the properties depend on variables that are solved, they must be defined by the user in a separate file called *ground.f*, which is a subroutine called by Earth. The file *ground.f* is discussed in the next section.

The second section of the Q1 file contains the boundary conditions. Examples of boundary conditions include the gas flux, enthalpy, velocity and species concentrations at the inlet, as well as the outer wall temperatures. These boundary conditions are represented as "sources," which are defined by the linear relation:

$$S_{\varphi} = C_{\varphi}(\varphi - V_{\varphi}) \tag{10}$$

where φ is the in-cell value of the variable in question, C_{φ} is the coefficient, and V_{φ} is the value. Both the coefficient and value are entered by the user to obtain the correct source term, which is added to the balance equations for the particular variable.

In the simplest case, S_{φ} is set to zero. This corresponds to cases of fixed boundary conditions, such as inlet velocities. With the source set to zero, the parameter φ is forced to be equal to the user-specified value V_{φ}. For example, suppose that the desired boundary condition is to set a particular velocity, U1, to 100 *m/sec* at the inlet. With φ = U1, and by setting the coefficient C_{U1} to zero and the value V_{U1} to 100 m/sec, the source equation becomes $S_{U1} = 0 \times (U1 - 100\frac{m}{s}) = 0$. Since the source term equals zero, the velocity U1 is set to the value V_{U1}. Thus, $U1 = 100$ *m/sec.*

In most cases, the coefficient and value are the results of other equations, such as chemical reaction models, etc., and are therefore computed in *ground.f*. For these complex

boundary conditions the source does not equal zero, and is therefore added to the proper balance equation. Examples of the more complicated sources include those used to set the concentrations of the species after each reaction at the growth surfaces. (See Appendices B and C for more details.)

Finally, the third section of the Q1 code determines both the criterion for the completion of a run and the format of the output ASCII file. It limits the number of iterations allowed, and determines the maximum residual accepted for convergence. In addition, the user may specify which variables are to be displayed in the final output file.

2.4.2.2 Earth

The main flow simulator is contained in the Earth code. The equations representing the physical laws and properties are encoded in this program. While PHOENICS can solve for simple phenomena such as velocity and enthalpy, the user must write code to solve for more complex phenomena such as heat transfer through different regions and chemical reactions. As mentioned above, any physical properties that rely on solved variables, such as specific heat or density, must be encoded by the user in *ground.f.* Since the furnace requires a relatively complex model, almost all of the properties contained in the model have been encoded in *ground.f.*

The output of Earth consists of two files: (1) RESULT -- an ASCII file that displays the final values of the solved variables, the residuals for each iteration, and the net source values entered, and (2) PHIDA -- a binary file containing the solutions to the variables that can be read by the post-processor Photon, which is described in the next section.

The order of execution is as follows. The interpreted Q1 file from Satellite is executed by Earth. If the Q1 file calls for information found in *ground.f*, Earth executes the corresponding FORTRAN segments. Since we did not have access to the source code, it was

particularly difficult to determine how the code written by the user was incorporated into the overall flow equations.

2.4.2.3 Photon

Photon is an interactive code that reads the PHIDA file from Earth and graphically displays the output on the screen in an Xwindow environment. It can display both two- and three-dimensional vector and contour plots. The graphics capabilities were especially useful for visualizing the results of the three-dimensional simulations. Examples of graphics created by Photon can be found in Chapter 5. Figure 1 shows a schematic of the overall relationship among Satellite, Earth, and Photon.

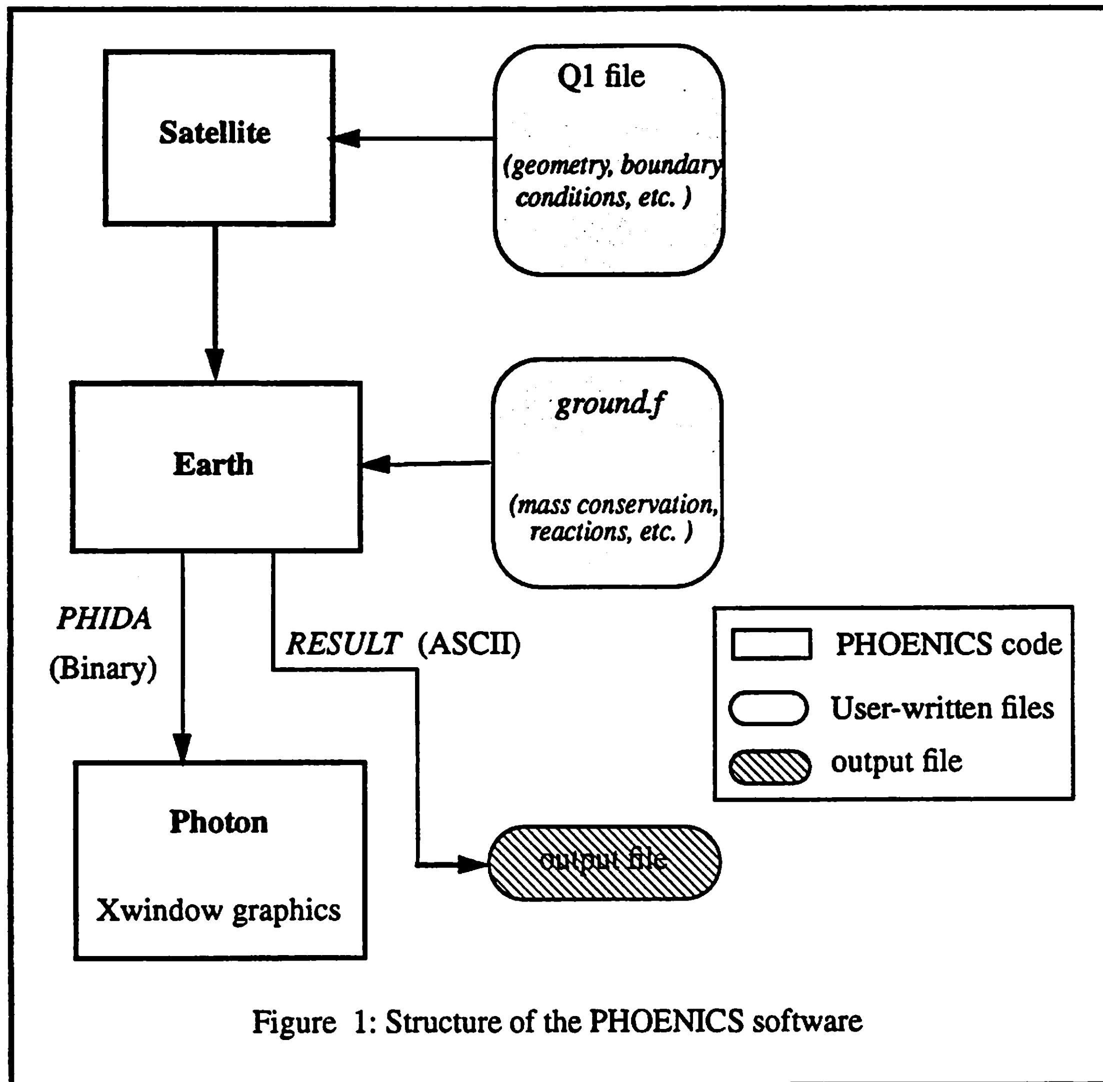

Figure 1: Structure of the PHOENICS software

Chapter 3 LPCVD Furnace Model

This chapter describes the actual furnace used for deposition and the computer model derived to simulate it. The model relies on equations which describe phenomena such as fluid flow, mass transport, heat transfer, etc. An explanation of the properties relevant to the model is given below. The coding for the chemical reactions is rather complex; it will be discussed in the following chapter.

3.1 Model Parameters

Within the simulator, several parameters interact with physical relations. These parameters can be grouped into equipment, process, and performance parameters [14]. Equipment parameters determine the equipment design of those constraints which can not be altered by the process engineer during routine processing. For the LPCVD case, equipment parameters define the geometry of the furnace, which includes the chamber size, position and size of the wafers and heat baffle, and the dimension of the inlet. In contrast, process parameters, such as temperature, pressure, inlet gas flux, and time of deposition, can be controlled by the process engineer. The equipment and process parameters, in conjunction with the fundamental laws discussed in the previous chapter, determine the performance parameters, which include thickness, across and within wafer uniformity, resistivity, and stress. The goal of this project is to build a model that will predict wafer thickness and uniformity. Resistivity and stress simulations will be performed in the future.

In the simulation software, the process parameters such as the furnace temperature and flux of the inlet gas species are entered through boundary conditions. Other physical constants are also required, such as viscosity, gas density, thermal conductivity, and diffusion

coefficients. The following sections describe the equipment parameters and the physical relations used in the model.

3.2 Furnace Description

Figure 2 depicts the Tylan horizontal glass tube reactor used for undoped polysilicon LPCVD. The wafers are stacked perpendicularly to the axis in the center of the tube, and are placed 1.2 cm apart. Aluminum cantilever rods support the boats, which house the wafers. Our simulations do not include effects of the cantilever rods or the boats. Other simulations, however, have shown that they contribute to a slightly more uniform growth [15]. Silane is injected at the lower front end of the tube, and is pumped out from the back end[1]. Three main heating coils on the exterior of the tube maintain the proper operating temperature. A heat baffle in the front portion of the furnace reduces the radiative heat loss and also serves to create both a uniform temperature and velocity in the mid and back sections of the tube.

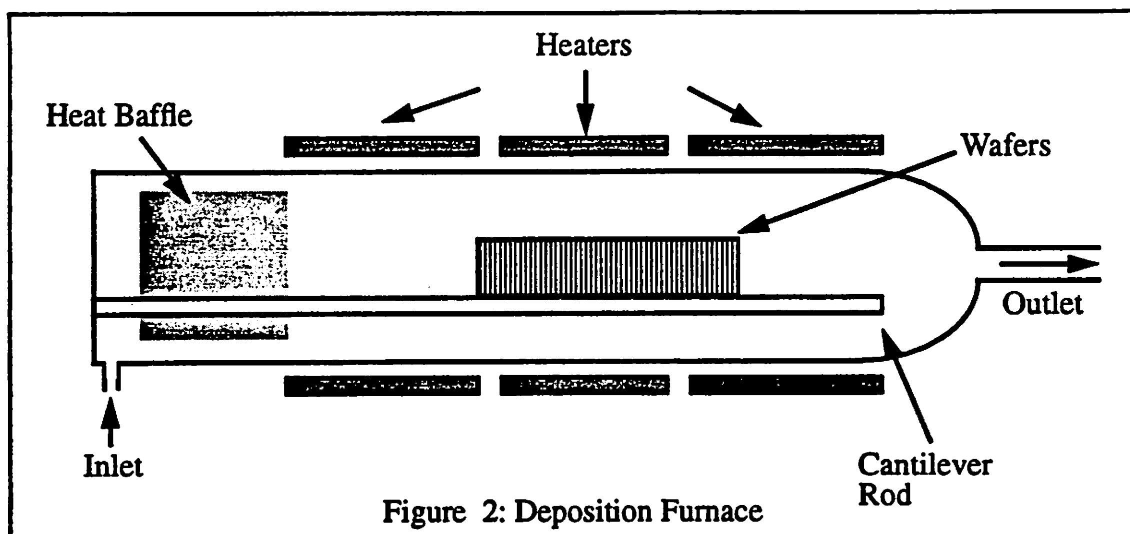

Figure 2: Deposition Furnace

1. Athough our actual furnace uses 100% silane injection at the inlet, the model can simulate inlet gases that are diluted with an inert carrier gas, such as argon or nitrigen.

3.3 Temperature Calculation

PHOENICS uses the conservation laws discussed in Chapter 2 to find the enthalpy of the material at any given point in the simulation grid. Temperature is then calculated using the following relationship between enthalpy H and absolute temperature T. This relationship depends upon the specific heat of each species:

$$T = \frac{H}{\sum_{i=1}^{k} w_i C_{P_i}(T)} \tag{11}$$

where H is the enthalpy in *J*, w_i are the mass fractions of species *i*, and C_{pi}, are the specific heats of species *i* in *J/(kgK)*. For undoped polysilicon deposition, the three species modeled are silane (SiH_4), hydrogen (H_2), and silene (SiH_2). Their balance as described by the w_i coefficients is calculated based on the detailed description of the chemical kinetics in Chapter 4.

As indicated in Eq. (11), the specific heat of each species is a function of temperature. An empirical fit for the specific heat of the gases in the model was found in the literature [8], which follows the form:

$$\frac{C_P(T)}{R} = a_i + b_i T + c_i T^2 + d_i T^3 + e_i T^4 \qquad , i = 1...k \tag{12}$$

The constants a, b, c, d, and e are characteristic of the particular gas, and temperature T is in degrees Kelvin. Published values were used for the specific heats for silane, silene, and hydrogen [8], which can be found below in Table 2.

Since Eq. (11) is non-linear in temperature, an iterative process is used to calculate the temperature of each cell. First, an estimated temperature is used in Eq. (12) to calculate an estimated specific heat. This value is then used in Eq. (11). If the resulting temperature is not equal to the temperature used in Eq. (12), the average of the two temperatures is found. The above steps are then repeated, this time using the average temperature as the initial

temperature in Eq. (12). This process continues until Eq. (11) and (12) converge to the same temperature.

	a	b	c	d	e
SiH_4	1.4516	0.12987E-1	-0.4234E-5	-0.2361E-8	0.1371E-11
SiH2	4.1082	-0.2386E-2	0.1224E-4	-0.1184E-7	0.3760E-11
H_2	2.9432	0.34815E-2	-0.7771E-5	0.74997E-8	-0.2520E-11

Table 2: Parameters for Specific Heat

As shown in Figure 3, the wafer region of the furnace can be abstracted into a cylinder, with both longitudinal (z) and radial (y) directions of flow. In the current model, we assume radial symmetry in the wafer region. Therefore, we can model a fraction of the radial dimension of the furnace for a complete solution. In future models, however, the effect of gravity will be included, which will invalidate the radial symmetry assumption. The next sections discuss the physical properties important in each direction of flow.

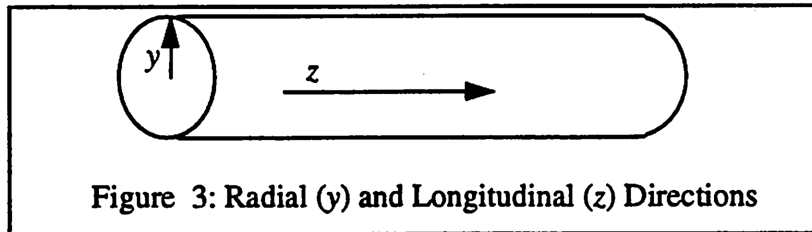

Figure 3: Radial (y) and Longitudinal (z) Directions

3.4 Longitudinal Flow

3.4.1 Reynold's Number

The Reynold's number of the system determines whether the flow can be considered laminar or turbulent. It is defined as the ratio of the inertia force over the viscous force:

$$Re = \frac{\rho v L}{\mu} \tag{13}$$

where v is the linear velocity (*cm/sec*), L is the length of interest (*cm*), μ is the viscosity (*kg/cm sec*), and ρ is the density (*kg/cm*^{3}). A Reynold's number of 1000 signifies a transition from laminar to turbulent flow. In our furnace example, with an inlet silane flow of about 120 *sccm*, 900 K, and 300 *mtorr*, the velocity is approximately 50 *cm/sec*. For a hot-wall reactor of length 130 *cm*, the corresponding Reynolds number is calculated to be around 10, which means that the flow in the tube can be modeled as laminar flow.

Since the species involved are gases and the laminar viscosity does not change much with pressure and temperature, the viscosity is treated as a constant. The gases in the furnace are at low enough pressures that the ideal gas law can be used. Thus, the density is defined as:

$$\rho = M\frac{P}{RT} \tag{14}$$

where M is the molecular weight (*kg/mole*), P is the absolute pressure (*Pascals*), T is the temperature (K), and R is the universal gas constant (8.314 *J/mole K*). When more than one gas is present, the molecular weight becomes a weighted average of the species molecular weights:

$$M = M_1X_1 + M_2X_2 + M_3X_3 + \dots \tag{15}$$

where M_i is the molecular weight and X_i is the molar fraction of species *i*.

3.4.2 Prandtl and Peclet Numbers

An important parameter in convective heat transfer is the Prandtl number, defined as the ratio of the molecular diffusivity of momentum over the molecular diffusivity of heat:

$$Pr = \frac{\mu Cp}{k} \tag{16}$$

where k is the thermal conductivity in *J/m sec K*, and μ and Cp are as previously defined. The Prandtl number is used extensively to model heat transfer from the gases through the

furnace walls, and through the heat baffle. The product of Reynolds and Prandtl numbers is the Peclet number,

$$Pe = RePr = \frac{\rho v L C p}{k} \tag{17}$$

which measures the relative importance of convection versus diffusion. When Pe >> 1, convection dominates, and when Pe << 1 diffusion dominates. For the furnace described above, the Peclet number is about 5 which indicates that in the longitudinal flow both convection and diffusion are important, and therefore both convection and diffusion must be modeled.

3.5 Radial Flow

3.5.1 Multicomponent Diffusion

Since the wafers are stacked vertically, the dominant radial flow mechanism between the wafers is through diffusion [4]. First, diffusion with two components will be discussed. Then the theory will be extended to cases with more than two components.

The flux resulting from diffusion can be derived from Fick's first law, which defines the diffusion component of A in an isothermal, isobaric system. For diffusion in the *z* (radial) direction,

$$J_{A,z} = -D_{AB}\frac{dc_A}{dz} \tag{18}$$

where $J_{A,z}$ is the molar flux in the *z* direction relative to the molar average velocity, $\frac{dc_A}{dz}$ is the concentration gradient in the *z* direction, and D_{AB} is the diffusion coefficient for component A diffusion through component B [16]. Therefore, according to Fick's law, a species can have a velocity relative to the average velocity of the mixture only if gradients in the concentration exist.

With some manipulation, the molar flux N_A (*mole/sec m*^{2}), relative to a stationary set of axes, can be written as:

$$N_A = -cD_{AB}\nabla y_A + y_A(N_A + N_B) \qquad (19)$$

where c is the total molar concentration (*mole/m*^{3}), D_{AB} is the diffusion coefficient of component A diffusing through component B (*m*^{2}*/sec*), and y_A is the mole fraction of component A. The first term in Eq. (19) is the molar flux resulting from the concentration gradient, while the second term is the molar flux resulting from the bulk motion of the fluid.

The Chapman-Enskog kinetic theory is used to calculate the diffusion coefficient D_{AB} for two gases A and B:

$$D_{AB} = 0.0018583\frac{\sqrt{T^3\left(\frac{1}{M_A} + \frac{1}{M_B}\right)}}{\Omega_{D_{AB}} P\sigma_{AB}^2} \qquad (20)$$

where D_{AB} is in cm^2/s; T is the absolute temperature in Kelvin; M_A and M_B are the molecular weights of species A and B in *kg/mole*; P is the absolute pressure in atmospheres; σ_{AB} is the collision diameter in Å; and Ω_D is a dimensionless function of the temperature and of the intermolecular potential field. Ω_D is related to the Lennard-Jones parameters σ_{AB} and ε_{AB} which are derived from viscosity data and have been tabulated [17]. The parameter ε_{AB} is the energy of molecular interaction for the binary system A and B in *ergs*. For a range of temperatures, the relationship of ε_{AB} and σ_{AB} to Ω_D can also be found in tables [17]. To calculate the values for a mixture of two gases, we use the standard approximations:

$$\sigma_{AB} = \frac{1}{2}(\sigma_A + \sigma_B) \qquad (21)$$

$$\varepsilon_{AB} = \sqrt{(\varepsilon_A \varepsilon_B)} \qquad (22)$$

Since silene (SiH_2) is an unstable compound, it is difficult to obtain values for the Lennard-Jones parameters. The values used in this model have been those estimated by Coltrin, *et al* [8]. The potential parameters for silene were obtained by linear interpolation

between the Lennard-Jones parameters of SiH and those of SiH_4, so that the values for silene are approximate. The values used in the model are listed in the following table.

Molecule	σ (Å)	ε/k (K)
SiH_4	4.084	207.6
SiH_2	3.803	133.1
H_2	2.968	33.3

Table 3: Potential Parameters

Gas mixtures comprising of more than two species have transport properties described by the diffusion coefficients for each pair in the mixture. Wilke [18] has simplified the Stefan-Maxwell equations presented by Hirschfelder, Curtiss, and Bird [19] to a close approximation, which is valid in dilute mixtures[1]. For a mixture with three gas species, the diffusion coefficient for species 1 in the mixture D_{1-mix} can be approximated by:

$$D_{1-mix} = \frac{1}{\frac{y'_2}{D_{1-2}} + \frac{y'_3}{D_{1-3}} + \dots + \frac{y'_n}{D_{1-n}}} \tag{23}$$

where D_{1-n} is the diffusion coefficient for the binary pair of species 1 diffusing through species n, and y'_n is the mole fraction of species n in the gas mixture without species 1:

$$y'_2 = \frac{y_2}{y_2 + y_3 + \dots + y_n} = \frac{y_2}{1 - y_1} \tag{24}$$

3.5.2 Thermal Diffusion

Thermal diffusion becomes important in regions of high temperature gradients. While large particles tend to remain in the cold regions, small, light particles diffuse into the hot

1. "Dilute" means that none of the species exists in the mixture by more than 80%.

regions. Although some authors [10] support the assumption that thermal diffusion is insignificant in hot-wall reactors because of small temperature gradients, others [8, 20, 21] have shown thermal diffusion to effect the species concentration and in general, reduce deposition rates by as much as 4%. In our current model, however, the effect of thermal diffusion is neglected.

Chapter 4 Chemical Kinetics

A complete LPCVD model must include the homogeneous and heterogenous reactions involved. For polysilicon deposition, however, not all of the intermediary reactions are known. So far, the largest number of species that has been modeled is seventeen, by Coltrin *et al* [8]. As more reactions are added to the model, the complexity and computational time increases. Because of unknown reaction mechanisms and rates, it is questionable as to whether or not the results are significantly improved when more reactions are included [10]. Therefore, only up to two reaction mechanisms are modeled in this simulation of undoped polysilicon deposition. This chapter will discuss in detail the reactions implemented in our model.

4.1 One-Step Reaction

The simplest reaction to model is the single-step surface reaction, in which silane gas is decomposed directly into deposited silicon and hydrogen gas. This reaction accounts for about 80% of the deposition at low pressures [22]:

$$SiH_4 \leftrightarrow Si_{(s)} + 2H_2 \quad (25)$$

The rate of reaction used in the model has been previously published by Roenigk and Jensen [6]:

$$\mathcal{R} = \frac{k_o exp\left(\frac{-E_A}{RT}\right) P_{SiH_4}}{1 + K_{H_2}\sqrt{P_{H_2}} + K_{SiH_4} P_{SiH_4}} \quad (26)$$

where E_A is the activation energy (*kcal/mole*), P_{SiH_4} and P_{H_2} are the partial pressures of silane and hydrogen (*mtorr*), and k_o (*mol/m*^{2} *sec mtorr*), K_{SiH_4} (*torr*$^{-1}$), and K_{H_2} (*torr*$^{-0.5}$) are constants.

As seen in the above equation, the reaction rate is exponentially dependent on the activation energy and the temperature T (K). It also depends on the partial pressures of both gases involved, silane and hydrogen. The value for the activation energy in the above reaction has already been determined in the literature [23].

The values of the constants k_o, K_{SiH_4}, and K_{H_2} were fitted to experimental data using a non-linear optimizer [24]. The objective function of the optimizer was the sum of the squared differences of the experimental vs. simulated deposition rates of 6 wafers per run, across three different recipes. (Due to long simulation times, only three recipes were used in the optimization. In the future, more recipes should be included.) The three recipes chosen have input conditions which span the input space of the three parameters: temperature, pressure, and inlet silane gas flow. The specific recipe settings and results are in Chapter 5.

Once the reaction rate is calculated by PHOENICS, the silicon deposition rate, in *nm/min*, can be calculated by the relation:

$$\text{Depo} = \mathcal{R} \times M_{Si} \times \left(\frac{60.0\ \text{sec}}{\text{min}}\right) \times \left(\frac{1\times10^9\ \text{nm}}{\text{m}}\right) \times \frac{1}{\rho_{Si}} \tag{27}$$

where M_{Si} is the molecular weight of silicon (*kg/mole*), ρ_{Si} is the density of silicon (*kg/m³*), and the constants 60.0 and 1.E9 are for unit conversions to minutes and *nm*, respectively.

The reaction rate also determines the flux Φ (*kg/m² sec*) of H_2 or SiH_4 that is formed or lost, respectively.

$$\Phi_{H_2} = 2\mathcal{R}M_{H_2}(1 + w_{Si}) \tag{28}$$

$$\Phi_{SiH_4} = -\mathcal{R}M_{SiH_4}(1 - w_{Si}) \tag{29}$$

where M_i is the molecular weight in *kg/mole* of species *i*, w_{Si} is the mass fraction of solid silicon deposited, and the reaction rate $\mathcal{R}$ is as defined above. Since solids are not modeled, the corrective term $(1+w_{Si})$ must be added to compensate for the solid silicon depos-

ited. Otherwise, a convective flux into the cell will occur [25] due to a violation of mass conservation. In other words, if the correction term were not added, there would be a net loss of mass equal to the mass of the solid silicon formed in the reaction. Notice that if the mass percentage of Si is small, the flux need not be corrected by much. If the mass percentage is large, however, the correction term is substantial.

4.2 Two-Step Reaction

The two widely recognized mechanisms for deposition are either surface or diffusion-controlled. Surface-controlled reactions occur when an excess amount of reactants are available for the reaction. In such a case, the reactions are controlled primarily by the temperature of the deposition surface. On the other hand, in a diffusion-controlled reaction the reactants are consumed as fast as they are supplied, so that the reaction is limited by the availability of the gases. Since it is much easier to control the temperature rather than the amount of gas striking the wafers, surface reactions are preferable to diffusion-controlled reactions. Low pressures in the furnace promote a large flux of reactants at the surfaces, thus creating surface-controlled reactions. This is one of the reasons polysilicon CVD is usually performed at low pressures.

The second reaction mechanism that can be modeled is surface-controlled deposition. It involves a two-step reaction, where the surface reaction occurs on all heated surfaces, while a volume reaction occurs elsewhere. In the volume reaction silane yields silene and gaseous hydrogen,

$$SiH_4 \leftrightarrow SiH_2 + H_2 \qquad (30)$$

and in the surface reaction, the silene in turn yields solid silicon and gaseous hydrogen.

$$SiH_2 \leftrightarrow Si_{(s)} + H_2 \qquad (31)$$

4.2.1 Volume Reaction

The volume reaction occurs in any region where the gases are allowed to flow. The unimolecular reaction is modeled with an Arrhenius reaction rate (*sec*$^{-1}$) of the form [25]:

$$\mathcal{K}_{vol} = A\exp\left(\frac{-E_A}{RT}\right) \tag{32}$$

where E_A is the activation energy, R is the universal gas constant, and T is the temperature in degrees Kelvin. The constant A (*sec*$^{-1}$) can be found empirically. The gas flux per volume, in *kg/(m*^{3}*sec)*, into each cell is calculated for each species:

$$\Phi_{SiH_4} = -\mathcal{K}_{vol} \times \rho_{SiH_4} \times X_{SiH_4} \tag{33}$$

$$\Phi_{H_2} = \mathcal{K}_{vol} \times \rho_{H_2} \times X_{SiH_4} \tag{34}$$

$$\Phi_{SiH_2} = \mathcal{K}_{vol} \times \rho_{SiH_2} \times X_{SiH_4} \tag{35}$$

where $\mathcal{K}_{vol}$ is the rate calculated above, ρ is the density of the particular species in *kg/m*^{3}, and X_{SiH_4} is the mole fraction of silane. Notice that the flux of silane is negative while the flux of hydrogen and silene are positive, denoting a loss of silane and generation of hydrogen and silene.

4.2.2 Surface Reaction

The surface reaction occurs on all heated surfaces, including wafers, reactor walls, cantilever rods, and the boat. The surface reaction rate $\mathcal{K}_{sur}$ (*mole/m*^{2}*sec*) depends on the mole fraction of silene that reaches each grid surface area, along with the pressure and temperature [25].

$$\mathcal{K}_{sur} = 6.64P\sqrt{T}\frac{X_{SiH_2}}{RT} \tag{36}$$

The silicon deposition rate, in *nm/min*, can again be calculated by the relation:

$$\text{Depo} = \mathcal{K}_{sur} \times M_{Si} \times 60.0 \times \frac{1E9}{\rho_{Si}} \tag{37}$$

(M_{Si} is the molecular weight of silicon in *kg/mole*, ρ_{Si} is the density of silicon, and the constants 60.0 and 1.E9 are for unit conversions to minutes and *nm*, respectively.)

The reaction rate determines the flux Φ (*kg/m²sec*) of H_2 or SiH_2 that is formed or lost, respectively.

$$\Phi_{H_2} = \mathcal{K}_{sur} M_{H_2}(1 + w_{Si}) \tag{38}$$

$$\Phi_{SiH_2} = -\mathcal{K}_{sur} M_{SiH_2}(1 - w_{Si}) \tag{39}$$

where M is the molecular weight in *kg/mole*, w_{Si} is the mass fraction of solid silicon deposited, and $\mathcal{K}_{sur}$ is as defined above. As in the previous case with the one-step reaction, the corrective term $(1+w_{Si})$ must be added to compensate for the solid silicon deposited. This correction is needed to prevent a convective flux from occurring.

4.3 Phosphine-doped polysilicon

In-situ doped polysilicon deposition has become standard practice in the industry. Although several steps are saved by doping the layer while growing it, the uniformity and deposition rate suffer [26]. Therefore, a physical model of the process will be useful in determining the optimum settings for a particular furnace. We think that the model developed for undoped poly deposition can be modified to simulate doped poly deposition by adding in another surface chemical reaction [6]:

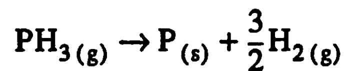

$$PH_{3\,(g)} \rightarrow P_{(s)} + \frac{3}{2}H_{2\,(g)}$$

Since the undoped poly deposition model can use two equations, it is relatively simple to add yet a third or fourth equation into the model. Each added equation, however, requires that additional parameters (i.e. reaction rate formulas and associated constants) be solved for empirically. These extra parameters will probably be the most difficult to obtain.

Chapter 5 Comparison with Actual Furnace

5.1 Introduction

The simulated data was compared against experimental data to test the applicability of the model. This chapter will compare the results of the experiments run in the Tylan 16 furnace in the Berkeley Microfabrication Laboratory with the results of the PHOENICS simulations of the furnace. Additionally, insight into important processes taking place inside the furnace will be discussed.

5.2 Experiments

5.2.1 Heat Baffle Temperature

The temperature profile in the Tylan 16 furnace was measured with a 16-point probe, which has thermocouples spaced 2.5" apart. The measurements show a large temperature ramp in the region of the heat baffle, from room temperature at the inlet to the deposition temperature in the growth region. As shown in Figure 4, the simulated temperature matches the actual furnace temperature quite well. Thus, the heat baffle serves as a good thermal insulator. In the following section, simulations show that the heat baffle also helps to create a more uniform gas flow in the wafer region.

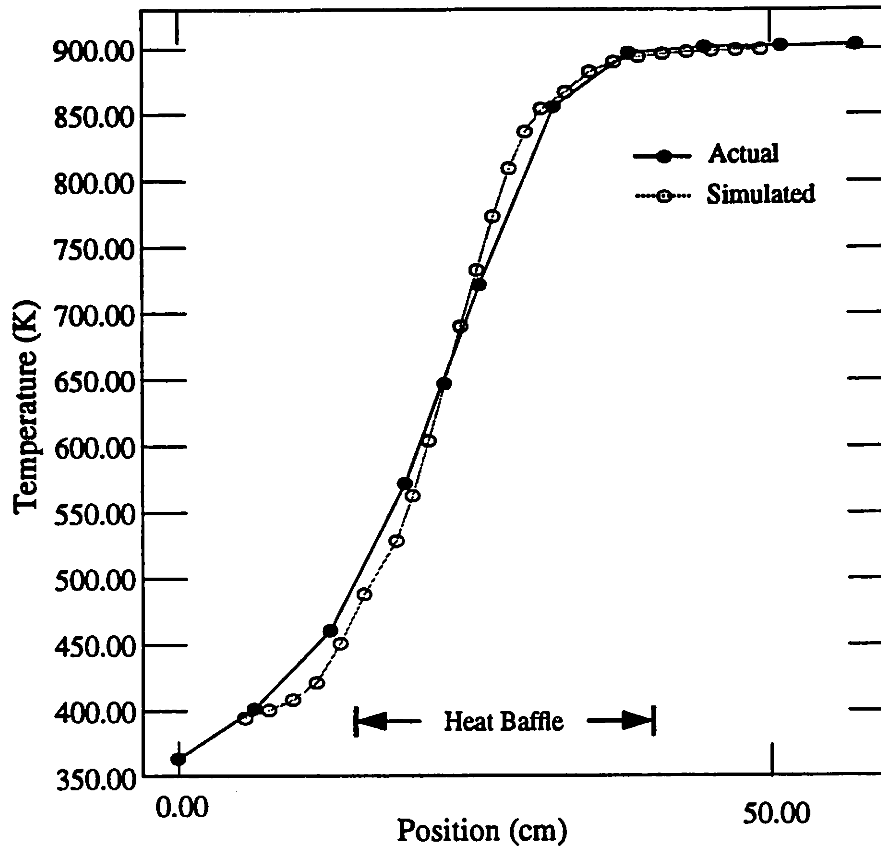

Figure 4: Temperature Profile in Heat Baffle Region

5.2.2 Wafer thickness and uniformity measurements

The experimental data of the Tylan furnace was obtained by Lin [3]. Twelve runs were performed, using a range of temperature, silane gas flow, pressure, and deposition time. In each of the runs, eight sample wafers were placed among eighteen dummy wafers, in positions 4, 7, 8, 9, 12, 17, 21, and 25 of the 26-slot boat. Each sample <111> wafer was covered with 1000Å of oxide. The deposition rate was measured at five points on each sample, at the center, and at each of the four corners. The thickness of the deposited silicon was measured with the Nanometrics NanoSpec AFT thickness measurement system, which was periodically calibrated using measurements collected with the more accurate AlphaStep 200 automatic step profiler. The deposition rate was computed as the average

of the thickness measurements divided by the deposition time. A summary of the experimental data is tabulated in Table 4. The rates shown in the table are those at the fourth wafer position, which is the set of wafers measured that was closest to the front of the tube.

Table 4: Experimental Data [3] vs. Simulated Results

Run #	T (°C)	P *(mtorr)*	Q *(sccm)*	time *(min)*	Rate *(Å/min)*
1	609	339	125	120	107.7
2	653	318	100	60	243.6
3	607	549	125	90	121.6
4	624	548	250	70	212.5
5	609	427	175	110	143.5
6	615	548	250	80	174.6
7	609	538	100	100	111.4
8	653	366	125	60	265.8
9	654	517	175	60	308.7
10	609	296	100	150	95.0
11	654	547	100	60	252.2
12	654	547	125	60	279.6

5.3 Simulated Undoped Polysilicon Deposition

5.3.1 Discretization of the Furnace Volume

As explained in Chapter 2, the furnace volume is discretized into cells, with regions of high gradients requiring more cells. When each wafer is modeled individually, the wafer region requires the most cells. While the detailed grid points in the wafer region do not unreasonably increase the simulation time in two-dimensions, in three-dimensions they add significant simulation time. (See Table 1 for exact simulation times). This section dis-

cusses a method to implement the wafers which reduces the number of grid points required. Both the two and three-dimensional grids used for the simulations are then depicted and discussed.

5.3.1.1 Discretization of the Wafer Region

Instead of modelling each individual wafer, a group of wafers is modeled as a "porous" region [27]. This means that in the wafer region, the gas velocities are restricted to flow only in the direction perpendicular to the flow. As can be seen in Figure 5, modelling a porous volume reduces the number of necessary grid points, thus decreasing the computational effort. Although modelling individual wafers results in more accurate gas velocities, the deposition rates are not affected by the volume reaction in the porous region. A few single wafers were included around the porous wafers to ensure that the conditions on the porous wafers were correct. As explained in Chapter 4, corrections to the mass flux due to the solid silicon deposition are made in the code.

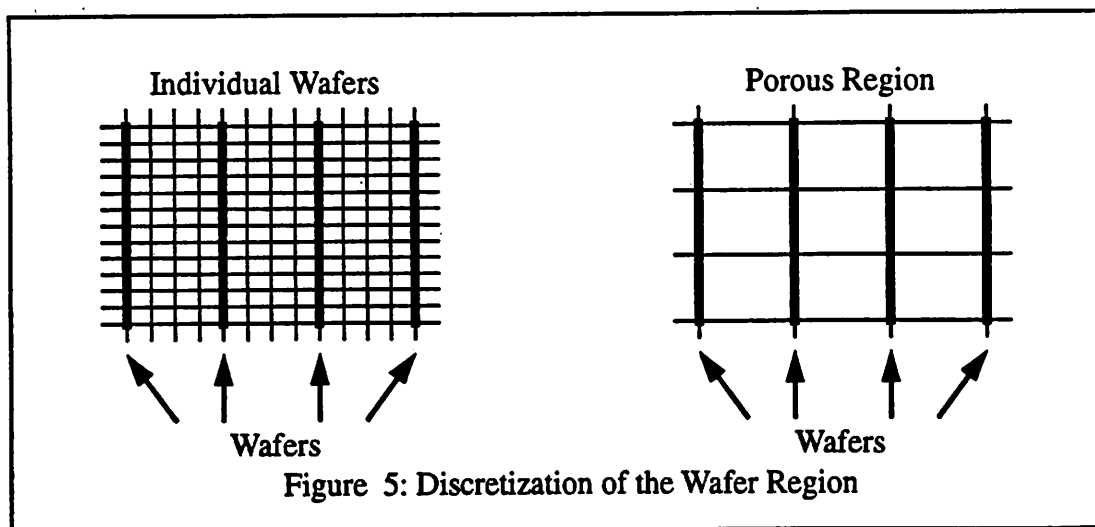

Figure 5: Discretization of the Wafer Region

5.3.1.2 Grid

The salient points of the grid used for the two-dimensional simulations are shown in Figure 6. The features of interest are the walls, the heat baffle, and the wafers. Of course

the grid extends throughout the entire furnace region; only the regions with actual physical structure are shown in Figure 6. Notice that a portion of the grid in the wafer region has very small grid spacings. These areas correspond to the regions that model the individual wafers, making it apparent that the porous regions indeed require fewer grid points. Other areas of high gradients, such as the inlet region, and the volume around the heat baffle, also have smaller grid spacings for more accurate results. On the other hand, regions of fairly uniform flow, such as the volume between the heat baffle and the wafers, require fewer grid points.

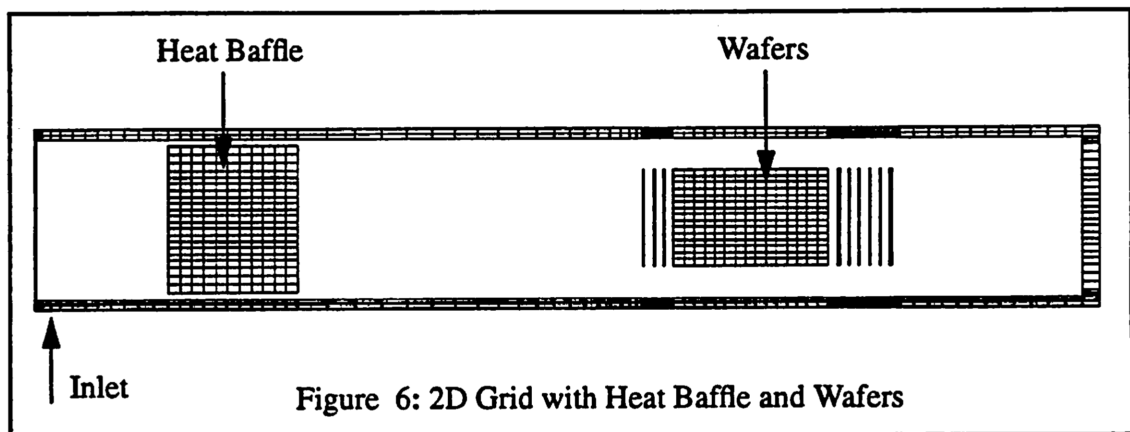

Figure 6: 2D Grid with Heat Baffle and Wafers

The inlet region can not be accurately modeled in just two-dimensions because the third dimension is unconstrained. Thus, for an accurate simulation, the full furnace must be modeled in three-dimensions. The three-dimensional simulation does not include individual wafers, as they would require far too much simulation time. Therefore, the porous wafers are used for all 26 wafers, as shown in Figure 7.

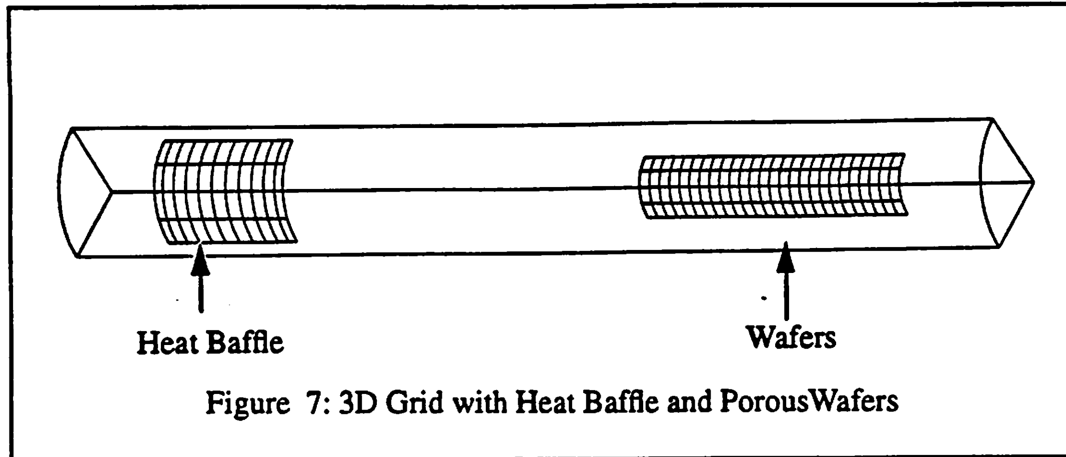

Figure 7: 3D Grid with Heat Baffle and PorousWafers

5.3.2 Gas Velocities

Figure 8 shows the gas velocity vectors in the front portion of the tube, including the inlet and heat baffle regions. The flow is laminar, indicated by the smaller velocities at the walls and larger velocities near the center of the tube. As the gas moves through the narrow region between the wall and the heat baffle, the velocity increases, due to the smaller cross-sectional area. It is clear from the figure that in addition to acting as an insulator, the heat baffle also serves to make the gas velocity more uniform around the heat baffle, so that the flow is uniform by the time it reaches the wafers. It might be interesting to investigate the benefits of differently-shaped heat baffles. For example, a baffle with curved edges could prevent the recirculation effects present at high inlet fluxes.

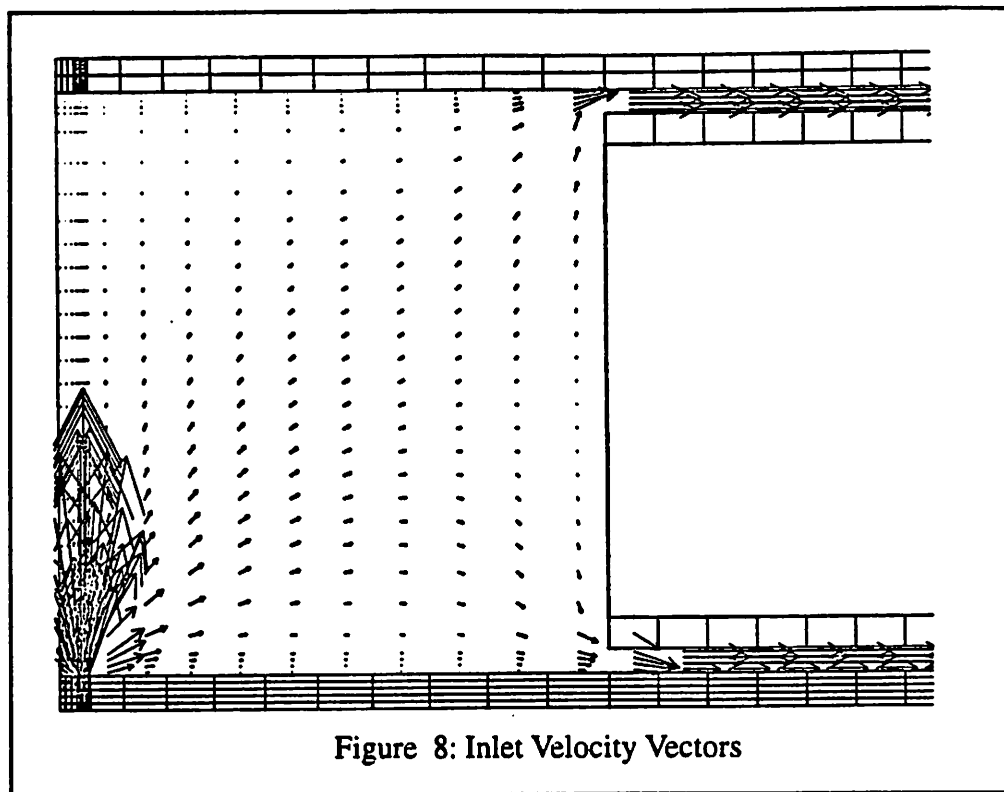

Figure 8: Inlet Velocity Vectors

Figure 9 shows a comparison between the gas flow among the wafers with and without surface reactions. (In all of the simulations, the one-step surface reaction was used in the model.) Note that the figure shows half of the region between wafers, with the edge of the wafer at the top of the figure. When there is no reaction present, the gases tend to recirculate between adjacent wafers as shown in Figure 9(a). One could surmise that this recirculation causes the higher depositions at the edges of the wafers. This is not a correct conclusion, however, since as Figure 9(b) shows, the recirculation disappears once a reaction is present. Notice that the gas velocity vectors are larger near the edges of the wafers. As the gas moves toward the center of the wafer, the velocity vectors become smaller and smaller until they are zero. This diffusion contributes to the uneven deposition across wafers, not recirculation. As others have shown, temperature differences along the wafer also contribute to this non-uniformity [28]. However, some contend that the major effect is due to diffusive transport, and not the temperature differences across the wafer [10]. Fig-

ure 10 shows the simulated within wafer non-uniformity. There is about a 1% non-uniformity across a single wafer from the center to the edge. Notice that the wafers closer to the front of the furnace are more uniform across the wafer than those at the back. This effect is due to the depletion of silane and the need to diffuse through hydrogen to reach the center of the wafer [10, 29], which is discussed in the following section. (Comparison to the experimental results is tentative, since effects of gravity are not yet included in our model.)

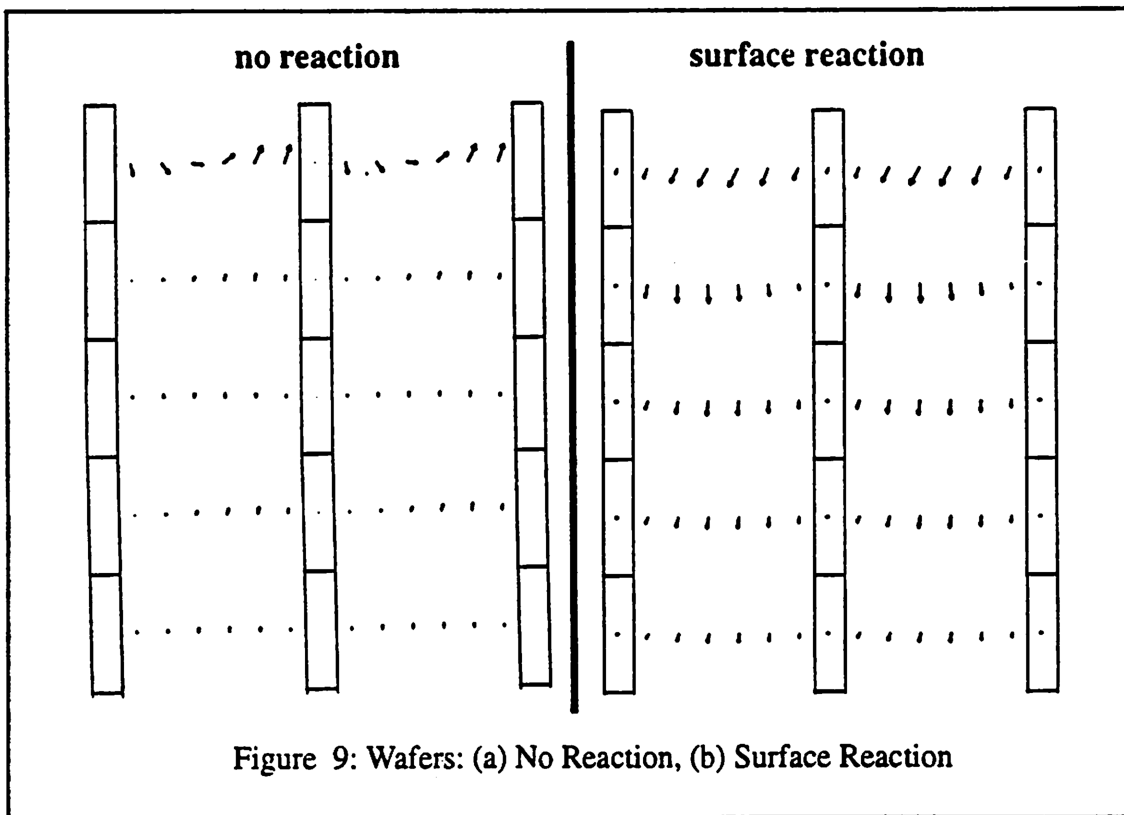

Figure 9: Wafers: (a) No Reaction, (b) Surface Reaction

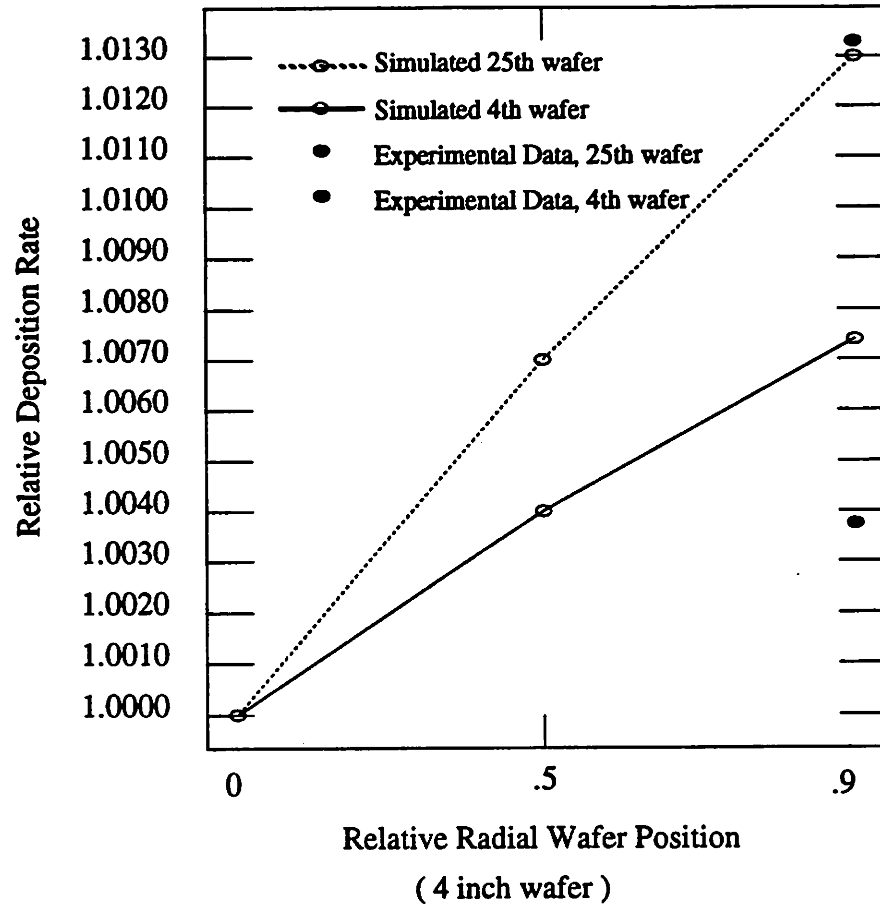

Figure 10: Within Wafer Non-uniformity

5.3.3 Concentration and Depletion Effects

As the silane reacts and forms solid silicon and gaseous hydrogen, the concentration of silane decreases as it flows along the tube, while the concentration of hydrogen increases. This dilution of silane with hydrogen causes the deposition rate to decrease along the tube. The depletion effect can be seen in Figure 11, which shows the contour plot of the decreasing concentration of silane. As shown in Figure 12, concentration gradients also exist across each wafer, which leads to the non-uniform deposition rate across the wafer.

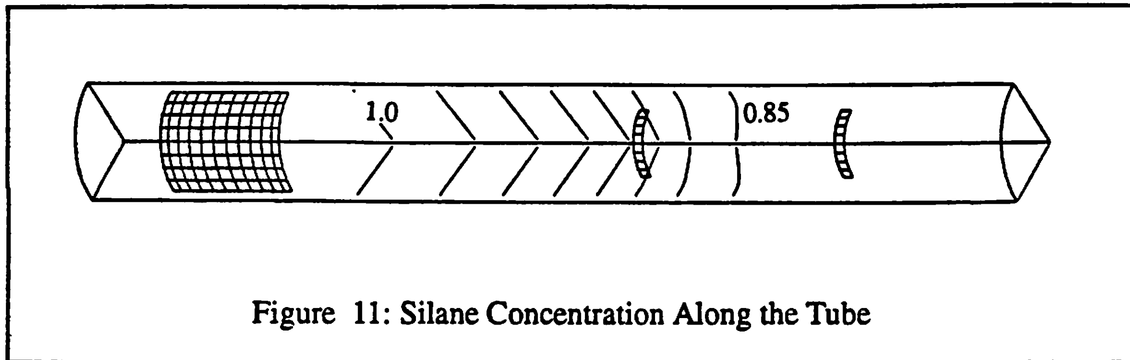

Figure 11: Silane Concentration Along the Tube

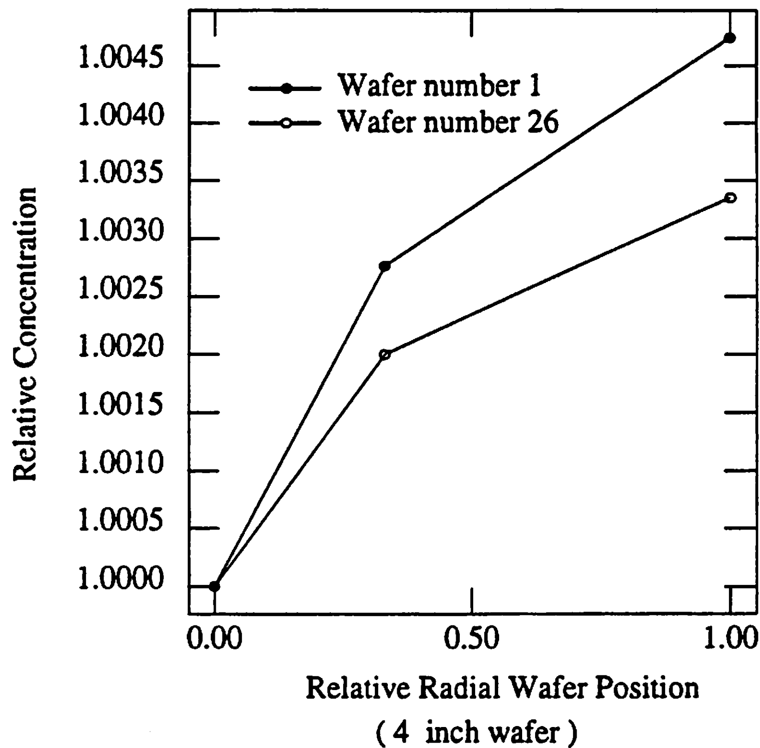

Figure 12: Silane Concentration Across Wafers

5.3.4 Deposition Rates

The results of the simulated versus experimental deposition rates are shown in Figure 13 for runs 1, 4, and 7. The standard deviation on the experimental data varies from 0.5 to

1.0 *Å/min* for runs 1 and 7, to 4.3 to 15.6 *Å/min* for run 4, as shown in Figures 14, 15, and 16. The model successfully predicts the general shape of the deposition profiles, with only an average error of 3.6% in the prediction of mean growth rate. The values used for the constants in Eq. (24) are tabulated in Table 3. Note that the values found by the otimizer are different from those published by Roenigk and Jensen [6]. The activation energy is 36.73 *kcal/mole*, which is consistent with other published literature [6, 20, 21, 26].

Table 5: Reaction Rate Constants

parameter	This model	Roenigk
k_o *mole/(m² sec mtorr)*	3.998435E4	1.579E4
K_{H2} $torr^{-0.5}$	1.418412	0.18849
K_{SiH4} $torr^{-1}$	4.893583E-2	0.6908

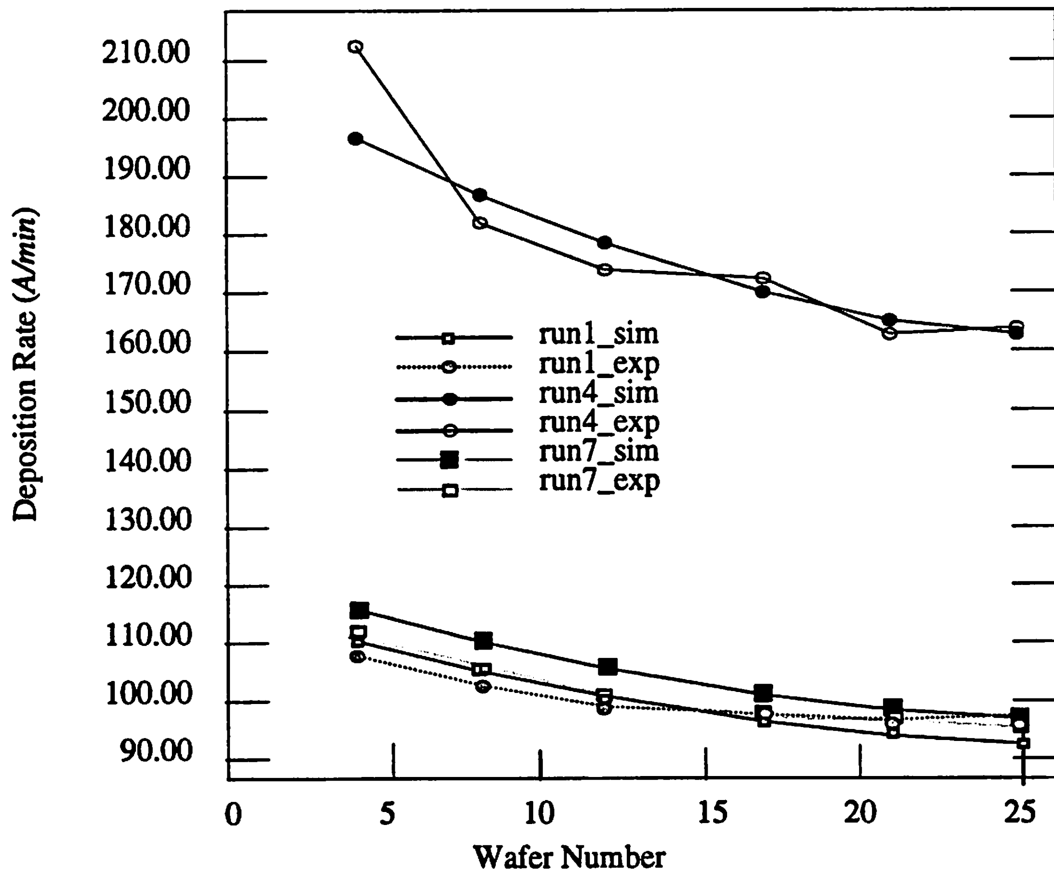

Figure 13: Simulated vs. Experimental Deposition Rates

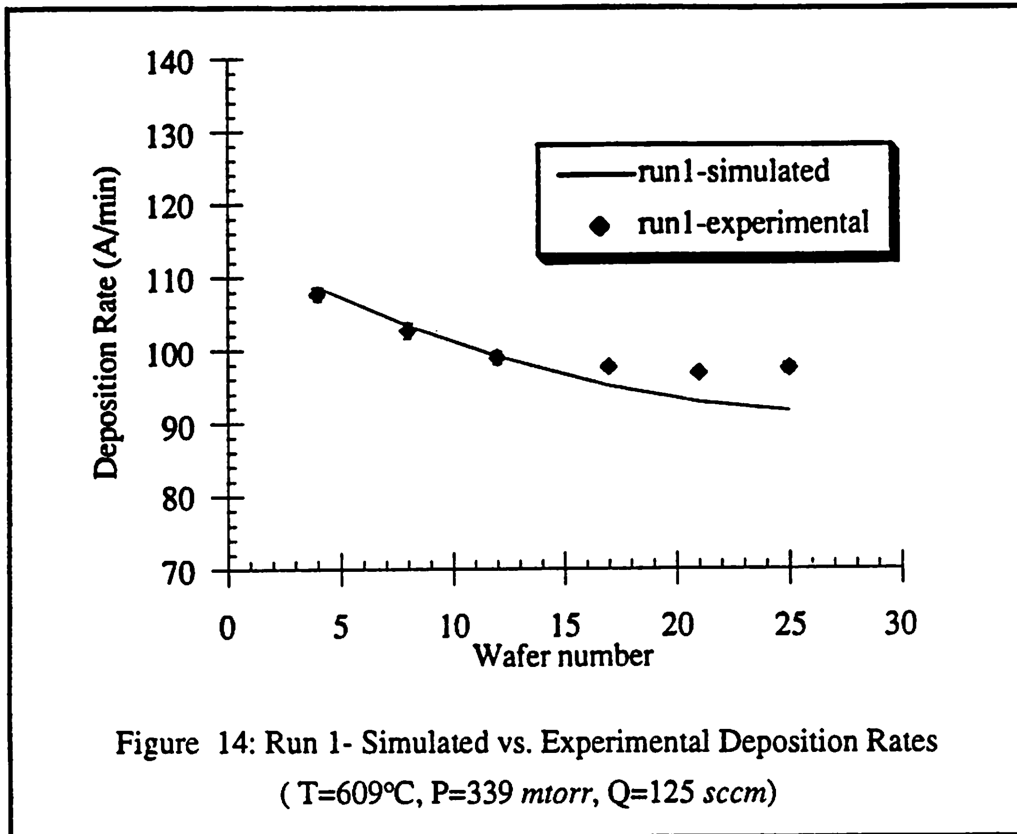

Figure 14: Run 1- Simulated vs. Experimental Deposition Rates
(T=609°C, P=339 *mtorr*, Q=125 *sccm*)

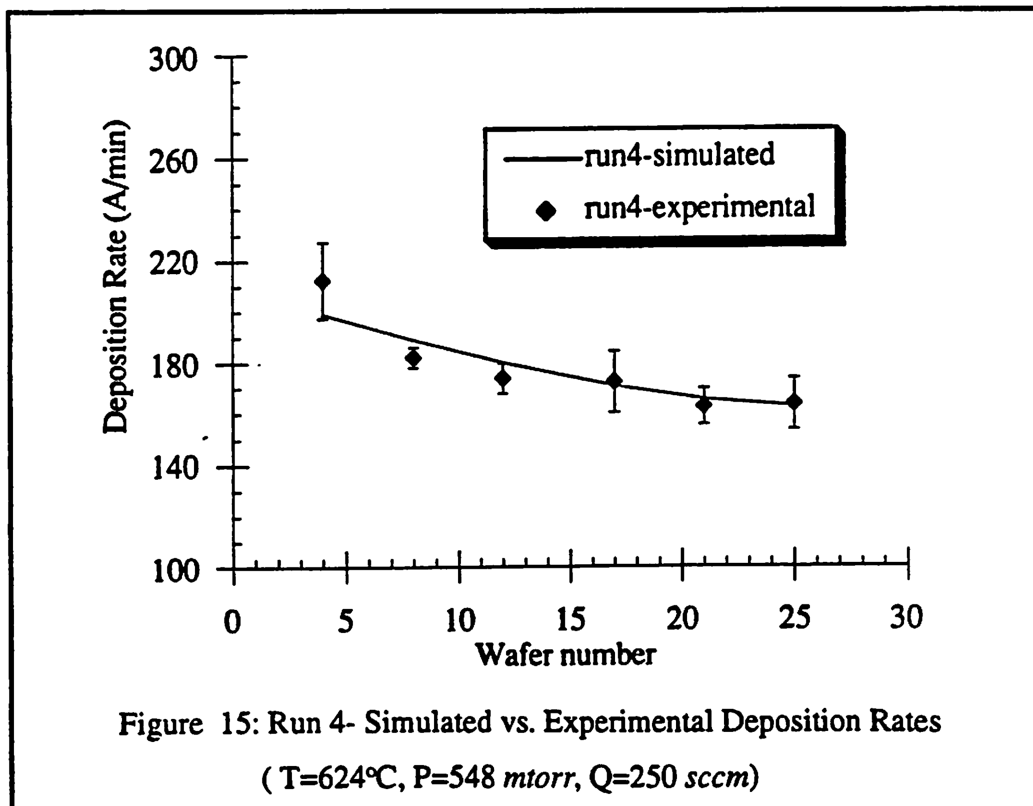

Figure 15: Run 4- Simulated vs. Experimental Deposition Rates
(T=624°C, P=548 *mtorr*, Q=250 *sccm*)

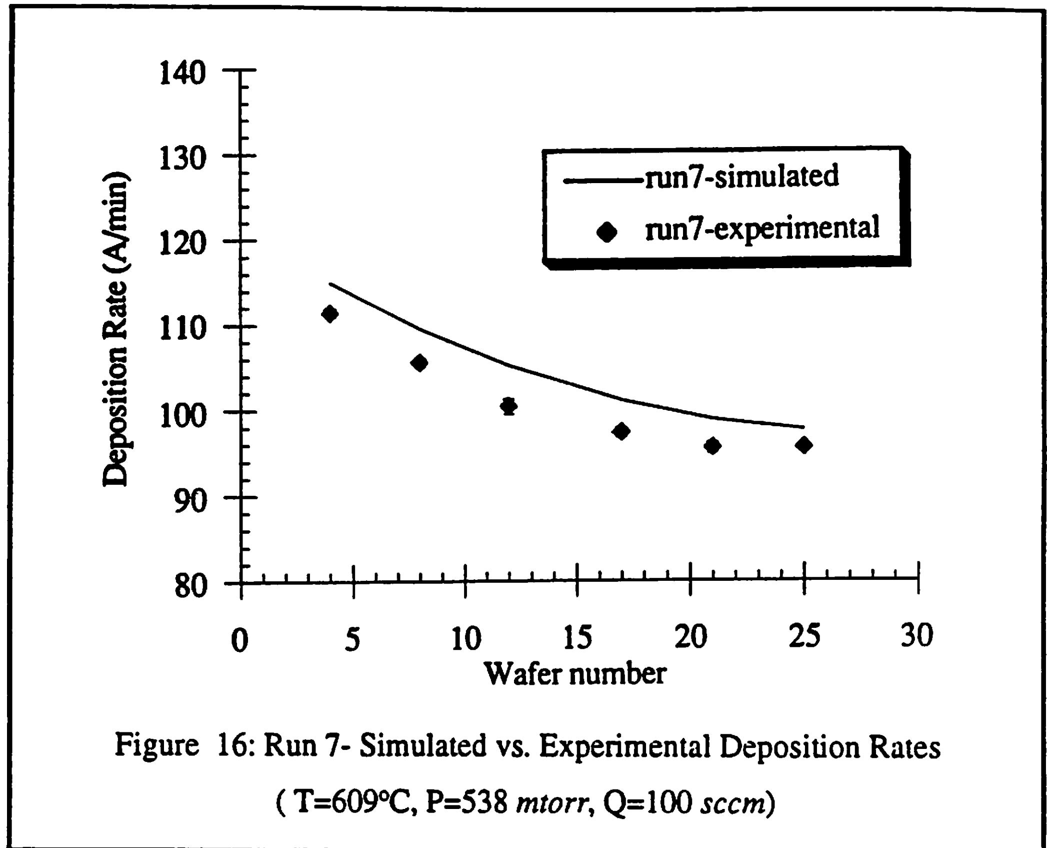

Figure 16: Run 7- Simulated vs. Experimental Deposition Rates
(T=609°C, P=538 *mtorr*, Q=100 *sccm*)

Chapter 6 Conclusions and Future Plans

Using the fundamental properties of fluid dynamics and chemical kinetics, we have developed a three-dimensional physical model of undoped polysilicon LPCVD. Given the input growth parameters of temperature, pressure, and input gas flow, the model predicts the wafer deposition rates along the length of a horizontal tube hot-wall furnace. The general profiles of across and within wafer uniformity have been in good agreement with experimental data, and the simulations have shown to be within 4% of the experimental mean values for a wide combination of temperature, pressure, and inlet gas flow settings.

The model has several potential applications. First, it can be used to optimize processes by the process engineer. Disturbances and small adjustments can be made to determine the most robust operating point [9]. Second, unlike empirical models, our physically-based model provides intuition about the phenomena inside the furnace, making it possible to study the effects of varying the pressure, temperature, and inlet gas flow on such properties as gas velocities, concentration gradients, and deposition rates. Third, the model can be used to help test different equipment designs, such as adding injectors along the furnace, or using a differently-shaped heat baffle. For example, adding injectors at carefully chosen spots down the length of the reactor may improve the longitudinal uniformity. Also, a heat baffle with curved edges might prevent recirculation effects. Fourth, although current CPU performance limitations do not allow for real-time applications, we also could use the model to help build a knowledge base to be used for diagnosis and control.

We believe that this model can serve as a framework for future models involving more chemical species, such as a model for doped polysilicon deposition. Additionally, the model can easily be adapted to study single-wafer equipment.

Appendix A: Nomenclature

Symbol	Meaning	Units
$\mathbf{a}$	acceleration (3-d vector)	m/sec^2
c	total molar concentration	$mole/m^3$
c_A	concentration of species A in equilibrium with the bulk composition of gas phase	$mole/m^3$
C_p	heat capacity	J/kg K
D_{AB}	mass diffusivity or diffusion coefficient for component A diffusing through component B	m^2/sec
F	force	N
$\mathbf{g}$	acceleration due to gravity (3-d vector)	m/sec^2
G_i	production rate of species *i* per unit volume	$kg/sec\ m^3$
H	enthalpy	J
J_i	molar flux of species *i* relative to the molar-average velocity	$mole/m^2$
$\mathbf{j}_i$	mass flux of species i relative to the mass average velocity	$kg/sec\ m^2$
k	thermal conductivity	W/m K
L	length	m
M_i	molecular weight of species i	kg/mole
N_i	molar flux relative to a set of stationary axes	$mol/sec\ m^2$
P	total pressure	Pa
q	heat flow rate	W
R	gas constant	$Pa\ m^3/mole\ K$
R_i	consumption rate of species i	$kg/sec\ m^3$
U	internal energy	$kg\ m^2/sec^2$
T	absolute temperature	K
$\mathbf{v}$	velocity	m/sec
w_i	mass fraction of species i	
Xi, y_A	mole fraction of species i, A	
ε	maximum attractive energy between two molecules	$kg\ m^2/sec^2$
μ	viscosity	Pa sec

ρ	density	kg/m^3
σ_{AB}	collision diameter	Å
τ	viscous stress tensor	kg/sec^3 m
Ω_D	collision integral	

Appendix B: PHOENICS Q1 File

The Q1 file is the PHOENICS CFD software input deck. The code used in the file consists of abbreviated calls to FORTRAN functions. Within the Q1 file is a description of the equipment parameters, such as reactor size and placement of the wafers. It contains the input boundary conditions such as inlet gas temperature, silane gas flow, and pressure. The file also contains commands which call the functions programmed in the *ground.f* file, such as density and heat conduction calculations, as well as the boundary conditions for the reactions on the wafers and reactor walls. The last few lines of the Q1 file determine the number of iterations to be performed and the convergence criteria.

The furnace geometry is defined in x, y, and z components, which refer to the azimuthal, radial, and axial directions of the reactor, repectively. Since the present model assumes radial symmetry, as discussed in Chapter 3, only 1/8 of the radial dimension of the furnace is simulated.

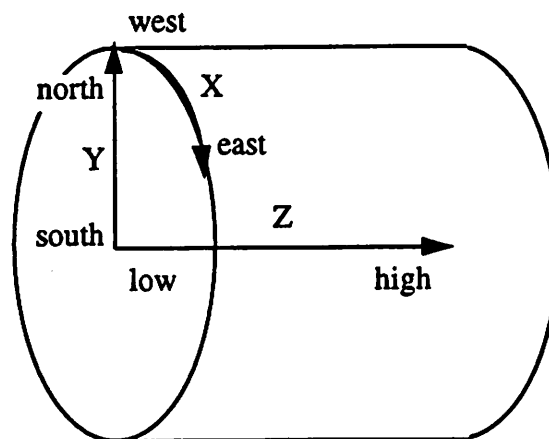

Each cell has six faces, the west, east, south, north, low, and high. The west and east faces correspond to the faces along the X direction, the north and south faces correspond to those along the Y direction, and the high and low face correspond to those along the Z direction.

```
TALK=F;RUN(1, 1);VDU=TTY
TEXT(RUN 7: 3-D model with Heat Baffle and Wafers)

          Declare Variables
REAL(TGAS,TWALL)

****************************************
          INPUT SETTING: Temperarure
****************************************
TGAS=320*823; TWALL=(605+273)*823

REAL (PRESSU,MWAVG,TAREA,MASFLX)
REAL (M1FLO,M2FLO,M3FLO,M4FLO,M5FLO)
REAL (M1FLX,M2FLX,M3FLX,M4FLX,M5FLX)
REAL (X1FLX,X2FLX,X3FLX,X4FLX,X5FLX)
REAL (M1FRAC,M2FRAC,M3FRAC,M4FRAC,M5IFLX)
REAL (TMPIN,RHOINL,SUM1,SUM2,XX1,XX2,XX3,XX4,XX5)
REAL (PI,T1,T2)

PI=3.14159265

          Steady-state simulation, with polar coordinates
STEADY=T
CARTES=F

**************************************************
          FURNACE DISCRETIZATION
**************************************************
          **** Azimuthal (X) Direction ****
INTEGER(KX1,KX2)
INTEGER(NXF01,NXL01,NXF02,NXL02)

KX1=2; KX2=2
NX=KX1+KX2
NXF01=1;NXF02=NXF01+KX1; NXL01=NXF02-1; NXL02=NX

          ** Eighth of a cylinder
SUBGRD(X,NXF01,NXL01,0.7854/2,1.0)
SUBGRD(X,NXF02,NXL02,0.7854/2,1.0)

          **** Axial (Z) Direction ****
INTEGER(KZ0,KZ1,KZ2,KZ3,KZ4,KZ5,KZ6,KZ7,KZ8)

KZ0=5; KZ1=11;
KZ2=15
KZ3=3; KZ4=10; KZ5=10; KZ6=3; KZ7=6

NZ=KZ0+KZ1+KZ2+KZ3+KZ4+KZ5+KZ6+KZ7

INTEGER(NZF00,NZL00,NZF01,NZL01,NZF02,NZL02,NZF03,NZL03)
INTEGER(NZF04,NZL04,NZF05,NZL05,NZF06,NZL06)
INTEGER(NZF07,NZL07,NZF08,NZL08,NZF09,NZL09)

NZF00=1
NZF01=NZF00+KZ0
NZF02=NZF01+KZ1;
NZF03=NZF02+KZ2; NZF04=NZF03+KZ3
NZF05=NZF04+KZ4; NZF06=NZF05+KZ5; NZF07=NZF06+KZ6

NZL00=NZF01-1
NZL01=NZF02-1;
NZL02=NZF03-1; NZL03=NZF04-1
NZL04=NZF05-1; NZL05=NZF06-1; NZL06=NZF07-1
NZL07=NZ

          ** Regions **
          Region 1: Heat Baffle
          Regions 3-6: Wafers
          Other regions: Gas

          Note that the coordinates are in units of length (meters)
SUBGRD(Z,NZF00,NZL00,0.100,1.2)
SUBGRD(Z,NZF01,-NZL01,0.152,1.2)
SUBGRD(Z,NZF02,NZL02,0.41,-1.2)
SUBGRD(Z,NZF03,NZL03,0.036,1.0)
SUBGRD(Z,NZF04,NZL04,0.120,1.0)
SUBGRD(Z,NZF05,NZL05,0.120,1.0)
SUBGRD(Z,NZF06,NZL06,0.036,1.0)
SUBGRD(Z,NZF07,NZL07,0.132,1.2)

          **** Radial (Y) Direction ****
INTEGER(JY1,JY2,JY3,JY4,JY5,JY6,JY7)
JY1=3; JY2=3; JY3=1; JY4=1
NY=JY1+JY2+JY3+JY4

INTEGER(NYF01,NYL01,NYF02,NYL02,NYF03,NYL03)
INTEGER(NYF04,NYL04)

NYF01=1
NYF02=NYF01+JY1; NYF03=NYF02+JY2; NYF04=NYF03+JY3

NYL01=NYF02-1; NYL02=NYF03-1; NYL03=NYF04-1; NYL04=NY

SUBGRD(Y,NYF01,NYL01,0.0575,-1.2)
SUBGRD(Y,NYF02,NYL02,0.0205,1.0)
SUBGRD(Y,NYF03,NYL03,0.0070,1.0)
SUBGRD(Y,NYF04,NYL04,0.0050,1.0)

          Integers to be used in the ground.f file
IG(1)=NYF04
IG(2)=NYL02
IG(3)=NZF01
IG(4)=NZL01

          ***** Store and Solve Variables ****
STORE (RHO1,ENUL)
STORE (DEPO)
STORE (X1,X2,X3,X4)
STORE (C21)
NAME (C21)=TEMP
STORE (M1)

SOLVE(P1,U1,V1,W1)
SOLUTN(P1,Y,Y,Y,N,N,N)
SOLVE(H1)
SOLUTN(H1,P,P,P,P,P,Y)
SOLVE(M2,M3,M4)

          ** Number of Species involved **
          Maximum number is 10
IG(20)=4
          ** Physical Properties **
          The following real numbers will be used in ground.f
          to calculate the specific heat and diffusion coefficients
          of each species.
          Molecular properties:
          RG(30) = molar mass
          RG(31) = collision diameter, sigma (Angstroms)
          RG(32) = Lennard-Jones (Kelvin)
          heat capacity (per unit mass):
          Cp = a + b*T + c*T^2 + d*T^3 + e*T^4
          RG(33) = par a
          RG(34) = par b
          RG(35) = par c
          RG(36) = par d
          RG(37) = par e

          ARGON (M1)
RG(30)=40.0E-3
RG(31)=3.542
RG(32)=93.3
RG(33)=20.8/RG(30)
RG(34)=0.0
RG(35)=0.0
```

```
RG(36)=0.0

          SiH4 (M2)
RG(40)=32.12E-3
RG(41)=4.084
RG(42)=207.6
RG(43)=1.4516
RG(44)=0.13987E-1
RG(45)=-0.42345E-5
RG(46)=-0.23636E-8
RG(47)=0.13712E-11

          H2 (M3)
RG(50)=2.016E-3
RG(51)=2.915
RG(52)=38.0
RG(53)=2.9432
RG(54)=0.34815E-2
RG(55)=-0.77713E-5
RG(56)=0.74997E-8
RG(57)=-0.25203E-11

          SiH2 (M4)
RG(60)=30.101E-3
RG(61)=3.803
RG(62)=133.1
RG(63)=4.1082
RG(64)=-0.23863E-2
RG(65)=0.12247E-4
RG(66)=-0.11841E-7
RG(67)=-0.25203E-11

****************************************************
          INPUT SETTINGS: Pressure, Gas Flow
****************************************************
          ** Pressure is entered in PRESSU in units of mtorr **
          Conversion to Pascals: 1 Pa = 7.5 mtorr
PRESSU=540
PRESS0=PRESSU/7.5

          *** Input the inlet gases (sccm)
M1FLO=0.0
M2FLO=100.0
M3FLO=0.
M4FLO=0.

          TAREA= area of the annular region between the
          walls and heat baffle (m^2)
TAREA = 3.14159*(0.085-0.078)**2/8

          Convert sccm to kg/s (STP conditions)
M1FLX=M1FLO*RG(30)*1.013E5/(60.*8.314*298.*1.E6)
M2FLX=M2FLO*RG(40)*1.013E5/(60.*8.314*298.*1.E6)
M3FLX=M3FLO*RG(50)*1.013E5/(60.*8.314*298.*1.E6)
M4FLX=M4FLO*RG(60)*1.013E5/(60.*8.314*298.*1.E6)

          Convert kg/s to mole/s
X1FLX=M1FLX/RG(30)
X2FLX=M2FLX/RG(40)
X3FLX=M3FLX/RG(50)
X4FLX=M4FLX/RG(60)

          Total flux in kg/s
MASFLX=M1FLX+M2FLX+M3FLX+M4FLX

 Compute the Mass Fractions
M1FRAC=M1FLX/MASFLX
M2FRAC=M2FLX/MASFLX
M3FRAC=M3FLX/MASFLX
M4FRAC=M4FLX/MASFLX
RG(10)=M1FRAC
```

```
          Compute the Mole Fractions
XX1=X1FLX/(X1FLX+X2FLX+X3FLX+X4FLX)
XX2=X2FLX/(X1FLX+X2FLX+X3FLX+X4FLX)
XX3=X3FLX/(X1FLX+X2FLX+X3FLX+X4FLX)
XX4=1.0 - (XX1+XX2+XX3)

          Inlet gas temperature
TMPIN=TGAS

          Compute the inlet gas density (kg/m^3)
SUM1=XX1*RG(30)+XX2*RG(40)+XX3*RG(50)+XX4*RG(60)
RHOINI=PRESS0*SUM1/(8.31441*TMPIN)


          Call the groundf file to solve for
          density (RHO1)
          laminar viscosity (ENUL)
          prandtl number for the gases and heat baffle (PRNDTL(H1))
          diffusion effects (PRNDTL(M2), PRNDTL(M3), PRNDTL(M4))
RHO1=GRND
ENUL=GRND

PRNDTL(H1)=GRND
PRNDTL(M2)=-GRND
PRNDTL(M3)=-GRND
PRNDTL(M4)=-GRND

          **** Initial Conditions ****
FIINIT(M1)=M1FRAC; FIINIT(M2)=M2FRAC; FIINIT(M3)=M3FRAC
FIINIT(M4)=M4FRAC; FIINIT(H1)=TWALL

          ********************************
          BOUNDARY CONDITIONS
          ********************************
          **** INLET Boundary Conditions***
PATCH(INLET,LOW,1,NX,1,NYL03,1,1,1,1)
COVAL(INLET,P1,FIXFLU,MASFLX/TAREA)
COVAL(INLET,M2,ONLYMS,M2FRAC)
COVAL(INLET,M3,ONLYMS,M3FRAC)
COVAL(INLET,M4,ONLYMS,M4FRAC)
COVAL(INLET,H1,ONLYMS,300*823)

          **** OUTLET Boundary Conditions****
PATCH(EXIT1,HIGH,1,NX,1,NY,NZ,NZ,1,1)
COVAL(EXIT1,P1,FIXP,0.0)
COVAL(EXIT1,M2,ONLYMS,SAME)
COVAL(EXIT1,M3,ONLYMS,SAME)
COVAL(EXIT1,M4,ONLYMS,SAME)
COVAL(EXIT1,H1,ONLYMS,SAME)

          **** NORTH WALLS Boundary Conditions****
 Set the wall velocities to be zero, to model laminar velocity
PATCH(NORA,NWALL,NXF01,NXL02,NYF04,NYF04,1,NZ,1,1)
COVAL(NORA,U1,GRND2,0.0)
COVAL(NORA,W1,GRND2,0.0)
COVAL(NORA,V1,FIXVAL,0.0)

PATCH(ANOR,CELL,NXF01,NXL02,NYF04,NYL04,1,NZ,1,1)
COVAL(ANOR,U1,FIXVAL,0.0)
COVAL(ANOR,V1,FIXVAL,0.0)
COVAL(ANOR,W1,FIXVAL,0.0)

          **** Set different wall temperatures on north wall
          **** in region of heat baffle
PATCH(NST0,NORTH,1,NX,NYL04,NYL04,1,NZL00,1,1)
COVAL(NST0,H1,1/PRNDTL(H1),400*823)

PATCH(NST3,NORTH,1,NX,NYL04,NYL04,NZF01,NZF01,1,1)
COVAL(NST3,H1,1/PRNDTL(H1),450*823)

PATCH(NST4,NORTH,1,NX,NYL04,NYL04,NZF01+1,NZF01+1,1,1)
COVAL(NST4,H1,1/PRNDTL(H1),480*823)
```

```
PATCH(NST5,NORTH,1,NX,NYL04,NYL04,NZF01+2,NZF01+2,1,1)
COVAL(NST5,H1,1/PRNDTL(H1),530*823)

PATCH(NST6,NORTH,1,NX,NYL04,NYL04,NZF01+3,NZF01+3,1,1)
COVAL(NST6,H1,1/PRNDTL(H1),600*823)

PATCH(NST7,NORTH,1,NX,NYL04,NYL04,NZF01+4,NZF01+4,1,1)
COVAL(NST7,H1,1/PRNDTL(H1),650*823)

PATCH(NST8,NORTH,1,NX,NYL04,NYL04,NZF01+5,NZF01+5,1,1)
COVAL(NST8,H1,1/PRNDTL(H1),700*823)

PATCH(NST9,NORTH,1,NX,NYL04,NYL04,NZF01+6,NZF01+6,1,1)
COVAL(NST9,H1,1/PRNDTL(H1),750*823)

PATCH(NST10,NORTH,1,NX,NYL04,NYL04,NZF01+7,NZF01+7,1,1)
COVAL(NST10,H1,1/PRNDTL(H1),800*823)

PATCH(NST11,NORTH,1,NX,NYL04,NYL04,NZF01+8,NZF01+8,1,1)
COVAL(NST11,H1,1/PRNDTL(H1),870*823)

PATCH(NST12,NORTH,1,NX,NYL04,NYL04,NZF01+9,NZF01+9,1,1)
COVAL(NST12,H1,1/PRNDTL(H1),TWALL)

PATCH(NST13,NORTH,1,NX,NYL04,NYL04,NZF01+10,NZ,1,1)
COVAL(NST13,H1,1/PRNDTL(H1),TWALL)

        **** HEAT BAFFLE ****
        ** Set wall velocities to zero **
PATCH(NWA,NWALL,1,NX,NYL02,NYL02,NZF01,NZL01,1,1)
COVAL(NWA,W1,GRND2,0.0)
COVAL(NWA,V1,FIXVAL,0.0)
COVAL(NWA,U1,GRND2,0.0)

PATCH(LWA,LWALL,1,NX,NYF01,NYL02,NZF01,NZF01,1,1)
COVAL(LWA,W1,FIXVAL,0.0)
COVAL(LWA,U1,GRND2,0.0)
COVAL(LWA,V1,GRND2,0.0)

PATCH(HWA,HWALL,1,NX,NYF01,NYL02,NZL01,NZL01,1,1)
COVAL(HWA,W1,FIXVAL,0.0)
COVAL(HWA,U1,GRND2,0.0)
COVAL(HWA,V1,GRND2,0.0)

        ** Set blockage velocities to zero **
PATCH(HBAF,CELL,1,NX,NYF01,NYL02,NZF01,NZL01,1,1)
COVAL(HBAF,U1,FIXVAL,0.0)
COVAL(HBAF,W1,FIXVAL,0.0)
COVAL(HBAF,V1,FIXVAL,0.0)

        **** DEPOSITION, on WALLS and WAFERS ****
        Note that ground.f is called (via GRND) to solve for
        the boundary conditions for the deposition.
        The wafers are modeled as the west face of each cell.

        **** Deposition on Furnace Walls ****
PATCH(Q1WALLS,NORTH,1,NX,NYL03,NYL03,NZF02,NZ,1,1)
COVAL(Q1WALLS,P1,FIXFLU,GRND)
COVAL(Q1WALLS,M2,FIXFLU,GRND)
COVAL(Q1WALLS,M3,FIXFLU,GRND)

        **** Deposition on 26 Wafers ****
        ** 3 porous wafers **
PATCH(AWAF1,WEST,1,NX,NYF01,NYL01,NZF03,NZL03,1,1)
COVAL(AWAF1,W1,FIXVAL,0.0)

PATCH(WAF1A,WWALL,1,NX,NYF01,NYL01,NZF03,NZL03,1,1)
COVAL(WAF1A,W1,FIXVAL,0.0)
COVAL(WAF1A,U1,GRND2,0.0)
COVAL(WAF1A,V1,GRND2,0.0)

PATCH(Q1A1W,WEST,1,NX,NYF01,NYL01,NZF03,NZL03,1,1)
COVAL(Q1A1W,P1,FIXFLU,GRND)
COVAL(Q1A1W,M2,FIXFLU,GRND)
COVAL(Q1A1W,M3,FIXFLU,GRND)

        ** 10 porous wafers **
PATCH(AWAF2,WEST,1,NX,NYF01,NYL01,NZF04,NZL04,1,1)
COVAL(AWAF2,W1,FIXVAL,0.0)

PATCH(WAF2A,WWALL,1,NX,NYF01,NYL01,NZF04,NZL04,1,1)
COVAL(WAF2A,W1,FIXVAL,0.0)
COVAL(WAF2A,U1,GRND2,0.0)
COVAL(WAF2A,V1,GRND2,0.0)

PATCH(Q1A2W,WEST,1,NX,NYF01,NYL01,NZF04,NZL04,1,1)
COVAL(Q1A2W,P1,FIXFLU,GRND)
COVAL(Q1A2W,M2,FIXFLU,GRND)
COVAL(Q1A2W,M3,FIXFLU,GRND)

        ** 10 porous wafers **
PATCH(AWAF3,WEST,1,NX,NYF01,NYL01,NZF05,NZL05,1,1)
COVAL(AWAF3,W1,FIXVAL,0.0)

PATCH(WAF3A,WWALL,1,NX,NYF01,NYL01,NZF05,NZL05,1,1)
COVAL(WAF3A,W1,FIXVAL,0.0)
COVAL(WAF3A,U1,GRND2,0.0)
COVAL(WAF3A,V1,GRND2,0.0)

PATCH(Q1A3W,WEST,1,NX,NYF01,NYL01,NZF05,NZL05,1,1)
COVAL(Q1A3W,P1,FIXFLU,GRND)
COVAL(Q1A3W,M2,FIXFLU,GRND)
COVAL(Q1A3W,M3,FIXFLU,GRND)

        ** 3 porous wafers **
PATCH(AWAF4,WEST,1,NX,NYF01,NYL01,NZF06,NZL06,1,1)
COVAL(AWAF4,W1,FIXVAL,0.0)

PATCH(WAF4A,WWALL,1,NX,NYF01,NYL01,NZF06,NZL06,1,1)
COVAL(WAF4A,W1,FIXVAL,0.0)
COVAL(WAF4A,U1,GRND2,0.0)
COVAL(WAF4A,V1,GRND2,0.0)

PATCH(Q1A4W,WEST,1,NX,NYF01,NYL01,NZF06,NZL06,1,1)
COVAL(Q1A4W,P1,FIXFLU,GRND)
COVAL(Q1A4W,M2,FIXFLU,GRND)
COVAL(Q1A4W,M3,FIXFLU,GRND)
***************************************************
        Number of iterations
LSWEEP=250
IG(15)=LSWEEP
 VARMAX(RHO1)=1E3
 VARMIN(RHO1)=-1E-7

        Limits on the Residuals
RESREF(P1)=1.0E-07
RESREF(U1)=1.0E-07
RESREF(V1)=1.0E-07
RESREF(W1)=1.0E-07
RESREF(H1)=1.0E-07

RELAX(U1,FALSDT,0.1)
RELAX(V1,FALSDT,0.1)
RELAX(W1,FALSDT,0.1)
RELAX(H1,FALSDT,0.5)

ECHO=T
RESTRT(ALL)

        Determine which variables to include in the RESULTS file
OUTPUT(TMP1,Y,N,N,N,N,N)
OUTPUT(W1,Y,Y,Y,Y,Y,Y)
OUTPUT(P1,N,Y,N,N,Y,Y)
```

```
YZPR=T; NYPRIN=NY/5; NZPRIN=5
NXPRIN=NX/5
TSTSWP=2
NPRINT=10000
STOP
```

Appendix C: PHOENICS *Ground.f* File

The *ground.f* file contains the functions called by the Q1 file. These include functions to compute temperature and density, as well as the boundary conditons for the chemical reactions on the walls and wafers. The main subroutines (written by the user) are contained in the following abbreviated *ground.f* file.

```
C**************************************************************
C SUBROUTINE GROUND
C*********************************************************
{ Declaration of arrays, variables, etc. are not shown.}
C*********************************************************

C * ** Calculations of TEMPERATURE, DENSITY, PRANDTL NO.,
C *** and DIFFUSION COEFFICIENTS ****

Retrieve the matrices that contain the values for M2, M3, and M4
(the mass fractions of silane, silene, and the inert gas, respectively)
CALL GETYX(LBNAME('M2'),GM2,JNY,JNX)
CALL GETYX(LBNAME('M3'),GM3,JNY,JNX)
CALL GETYX(LBNAME('M4'),GM4,JNY,JNX)

Retrieve the matrices that contain the values for P1 (pressure) and
H1 (enthalpy)
 CALL GETYX(P1,GP1,JNY,JNX)
 CALL GETYX(H1,GH,JNY,JNX)

C ****** Calculate the specific heat *******
C Read the constants from the Q1 file
 RN1=33
 RN2=34
 RN3=35
 RN4=36
 RN5=37

 DO 2000 INA=1,N
 A=RG(RN1+10*(INA-1))
 B=RG(RN2+10*(INA-1))
 C=RG(RN3+10*(INA-1))
 D=RG(RN4+10*(INA-1))
 E=RG(RN5+10*(INA-1))

 DO 2000 L=1,NX
 DO 2000 K=1,NY
 GCP(K,L)=
 1 ( A + B*GTMP1(K,L) + C*GTMP1(K,L)**2+
 1 D*GTMP1(K,L)**3 + E*GTMP1(K,L)**4 )
 GCP(K,L)= ( A + B*882 + C*882**2+
 1 D*882**3 + E*882**4 )

 For units of J/kg/K
 IF (INA .EQ. 1) GCP1(K,L)=GCP(K,L)*8.314/RG(30)
 IF (INA .EQ. 2) GCP2(K,L)=GCP(K,L)*8.314/RG(40)
 IF (INA .EQ. 3) GCP3(K,L)=GCP(K,L)*8.314/RG(50)
 IF (INA .EQ. 4) GCP4(K,L)=GCP(K,L)*8.314/RG(60)

 2000 CONTINUE


 DO 3000 I=1,NX
 DO 3000 J=1,NY

C ***** Prevent negative or zero mass fractions ****
 GM2(J,I)=AMAX1(1.E-20,GM2(J,I))
 GM3(J,I)=AMAX1(1.E-20,GM3(J,I))
 GM4(J,I)=AMAX1(1.E-20,GM4(J,I))

C ***** M1 is the same as at the inlet *****
 GM1(J,I) = M1FRAC
 GM1(J,I)=AMAX1(1.E-20,GM1(J,I))

C***** Calculate GM0: Mass of solid Silicon *****
 GM0(J,I) = 1. - (GM1(J,I)+GM2(J,I)+GM3(J,I)+GM4(J,I))
 GM0(J,I)=AMAX1(1.E-20,GM0(J,I))

C ***** Calculate molar fractions *****
 GX1(J,I)=1./(1+GM2(J,I)/GM1(J,I)*RG(30)/RG(40)+
 1 GM3(J,I)/GM1(J,I)*RG(30)/RG(50)+
 1 GM4(J,I)/GM1(J,I)*RG(30)/RG(60)+
 1 GM0(J,I)/GM1(J,I)*RG(30)/28.0855)

 GX2(J,I)=1./(1+GM1(J,I)/GM2(J,I)*RG(40)/RG(30)+
 1 GM3(J,I)/GM2(J,I)*RG(40)/RG(50)+
 1 GM4(J,I)/GM2(J,I)*RG(40)/RG(60)+
 1 GM0(J,I)/GM2(J,I)*RG(40)/28.0855)

 GX3(J,I)=1./(1+GM2(J,I)/GM3(J,I)*RG(50)/RG(40)+
 1 GM1(J,I)/GM3(J,I)*RG(50)/RG(30)+
 1 GM4(J,I)/GM3(J,I)*RG(50)/RG(60)+
 1 GM0(J,I)/GM3(J,I)*RG(50)/28.0855)

 GX4(J,I)=1./(1+GM2(J,I)/GM4(J,I)*RG(60)/RG(40)+
 1 GM1(J,I)/GM4(J,I)*RG(60)/RG(30)+
 1 GM3(J,I)/GM4(J,I)*RG(60)/RG(50)+
 1 GM0(J,I)/GM4(J,I)*RG(60)/28.0855)


C ***** Prevent negative concentrations *****
 GX1(J,I)=AMAX1(1.E-20,GX1(J,I))
 GX2(J,I)=AMAX1(1.E-20,GX2(J,I))
 GX3(J,I)=AMAX1(1.E-20,GX3(J,I))
 GX4(J,I)=AMAX1(1.E-20,GX4(J,I))

C ***** Start gas density calculation *****
 AMW=GX1(J,I)*RG(30)+GX2(J,I)*RG(40)+GX3(J,I)*RG(50)+
 1 GX4(J,I)*RG(60)

 HCPAVG=GX1(J,I)*GCP1(J,I)+GX2(J,I)*GCP2(J,I)+GX3(J,I)*GCP3(J,I)
 1 +GX4(J,I)*GCP4(J,I)

 IF (GTMP1(J,I) .GT. 950) GTMP1(J,I) = 950.
 IF (GTMP1(J,I) .LT. 300) GTMP1(J,I) = 300.

C ****** Calculation of Density *****
 GRH(J,I)=(GP1(J,I)+PRESS0)*AMW/(8.31441*GTMP1(J,I))

 3000 CONTINUE
```

```
CALL SETYX(DEN1,GRH,JNY,JNX)
CALL SETYX(TEMP,GTMP1,JNY,JNX)
CALL SETYX(LBNAME('X1'),GX1,JNY,JNX)
CALL SETYX(LBNAME('X2'),GX2,JNY,JNX)
CALL SETYX(LBNAME('X3'),GX3,JNY,JNX)
CALL SETYX(LBNAME('X4'),GX4,JNY,JNX)
CALL SETYX(LBNAME('M1'),GM1,JNY,JNX)

C In case the mass fractions are less than zero...
CALL SETYX(LBNAME('M2'),GM2,JNY,JNX)
CALL SETYX(LBNAME('M3'),GM3,JNY,JNX)
CALL SETYX(LBNAME('M4'),GM4,JNY,JNX)

RETURN
92 CONTINUE

C * ********** Calculation of Prandtl Number *******
IF (INDVAR .NE. H1) GOTO 999

DO 998 I=1,NX
DO 998 J=1,NY

LF=L0F(LAMPR) + J + NY*(I-1)

C Gaseous Region
F(LF) = 823*GENUL(J,I)*GDEN1(J,I)/0.0598

C Heat Baffle Region
IF ((IZ .GE. NZF01) .AND. (IZ .LE. NZL01) .AND. (J .LE. NYL02))
1 F(LF)=1800*GENUL(J,I)*GDEN1(J,I)/0.5

C Upper Wall
IF (J .GE. NYF04)
1 F(LF)= 1000*GENUL(J,I)*GDEN1(J,I)/1.0

998 CONTINUE

C ******** Calculation of the Diffusion Coefficients ********
C
C We need to calculate D2-mix, D3-mix, D4-mix
C This requires D2-3, D2-4, D3-4

999 SIGMA23 = 3.4995
SIGMA24 = 3.9435
SIGMA34 = 3.3590
C
C At 900K,
OMEGA23 = 0.7424
OMEGA24 = 0.8299
OMEGA34 = 0.7216

CALL GETYX(P1,GP1,JNY,JNX)
CALL GETYX(LBNAME('TEMP'),GTMP1,JNY,JNX)

C These values the same as those solved in RHO1.
CALL GETYX(LBNAME('X2'),GX2,JNY,JNX)
CALL GETYX(LBNAME('X3'),GX3,JNY,JNX)
CALL GETYX(LBNAME('X4'),GX4,JNY,JNX)

DO 8000 I=1,NX
DO 8000 J=1,NY

C Note that T is in Kelvins, P is atm, SIGMA in Angstroms, Molecular
C weights are in g/mole, OMEGA is unitless

D23(J,I)=0.001858*SQRT(1./(RG(40)*1.E3) + 1./(RG(50)*1.E3))
1 *GTMP1(J,I)**1.5/
1 ((PRESS0+GP1(J,I))*0.986923E-05*(SIGMA23**2)*OMEGA23)

D24(J,I)=0.001858*SQRT(1./(RG(40)*1.E3) + 1./(RG(60)*1.E3))
1 *900**1.5/
1 ((PRESS0+GP1(J,I))*0.986923E-05*(SIGMA24**2)*OMEGA24)

D34(J,I)=0.001858*SQRT(1./(RG(50)*1.E3) + 1./(RG(60)*1.E3))
1 *900**1.5/
1 ((PRESS0+GP1(J,I))*0.986923E-05*(SIGMA34**2)*OMEGA34)

GX23PR(J,I)=GX3(J,I)/(GX3(J,I) + GX4(J,I) + 1.E-20)
GX24PR(J,I)=GX4(J,I)/(GX3(J,I) + GX4(J,I) + 1.E-20)

GX32PR(J,I)=GX2(J,I)/(GX2(J,I) + GX4(J,I) + 1.E-20)
GX34PR(J,I)=GX4(J,I)/(GX2(J,I) + GX4(J,I) + 1.E-20)

GX42PR(J,I)=GX2(J,I)/(GX2(J,I) + GX3(J,I) + 1.E-20)
GX43PR(J,I)=GX3(J,I)/(GX2(J,I) + GX3(J,I) + 1.E-20)

8000 CONTINUE

DO 8001 I=1,NX
DO 8001 J=1,NY

C Solve for D2-mix, D3-mix, D4-mix

LAM=L0F(LAMPR) + J + NY*(I-1)
IF (INDVAR .EQ. LBNAME('M2'))
1 F(LAM) = 1.0E-4/(GX23PR(J,I)/D23(J,I) +
1 GX24PR(J,I)/D24(J,I))

IF (INDVAR .EQ. LBNAME('M3'))
1 F(LAM) = 1.0E-4/(GX32PR(J,I)/D23(J,I) +
1 GX34PR(J,I)/D34(J,I))

IF (INDVAR .EQ. LBNAME('M4'))
1 F(LAM) = 1.0E-4/(GX42PR(J,I)/D24(J,I) +
1 GX43PR(J,I)/D34(J,I))

8001 CONTINUE

8002 RETURN

C **************** DEPOSITION ***********************

C The coefficients A, Rh, and Rs are read in from a file
C called "coeff.in". The final deposition rates are written into
C a file called "depo.out."
C The subroutine that solves the chemical reaction is GDEP

open(4, file='coeff.in',status='old')
read(4,*) A, Rh, Rsi
close(4)

3040 CALL GDEP(A,Rh,Rsi,NPATCH,GVAL,GXX,GMM,GMW,-
F(L0TMP1+I),
1(F(L0P1+I)+PRESS0),N,F(L0DEPO+I),F(L0VAL+I))

open(3, file='depo.out',status='old')

IF ( ((ISWEEP .EQ. (SWEEP-1)).AND.(IX.EQ.2)).AND.(IY.EQ.1) ) THEN
IF (IZ.EQ.19) DEP4=F(L0DEPO+I)
IF (IZ.EQ.23) DEP8=F(L0DEPO+I)
IF (IZ.EQ.27) DEP12=F(L0DEPO+I)
IF (IZ.EQ.32) DEP17=F(L0DEPO+I)
IF (IZ.EQ.36) DEP21=F(L0DEPO+I)
IF (IZ.EQ.40) THEN
DEP25=F(L0DEPO+I)
write(3,*) DEP4,DEP8,DEP12,DEP17,DEP21,DEP25
close(3)
ENDIF

ENDIF

C*****************************************************************
```

```
C*************************************************************
C Subroutine GDEP: Solve the Chemical Reactions
C*************************************************************

 SUBROUTINE GDEP(A,Rh,Rsi,GPATCH,GVAR,GX,GM,GMW,GTEMP,
 1 GPRESS,GN,GDEPO,GFLX)

C ---------------------------

 DIMENSION GX(10),GM(10),GMW(10)
 REAL GTEMP,GPRESS,GDEPO,GFLX
 REAL GCON
 REAL A, Rh, Rsi
 INTEGER GVAR,GN
 CHARACTER GPATCH(8)

C ................
C Declaration of user variables

 REAL GR,K3,K4,KS,RS
 REAL GFLX1,GFLX2
 REAL RHOSI,MULT,MSI
 REAL P2,P3,Ea
C ................

 IF (GPATCH(1) .NE. 'Q') RETURN

C M1: Argon
C M2: SiH4
C M3: H2
C M4: SiH2
C M5: PH3 (not included here)

C
+++++++++++++++++++++++++++++++++++++++++++++++++++++++
C One-Step Reaction
C SiH4 --> Si(s) + 2H2
C
+++++++++++++++++++++++++++++++++++++++++++++++++++++++

 IF (GPATCH(2) .NE. '1') GOTO 1500

C Mass flows for chemical species into surface element [kg/(m^2s)]
C Density RHOSI: [kg/m^3]
C Molar mass of Si MSI: [kg/mole]

 RHOSI = 2.328E3
 MSI = 28.E-3

 PI = 3.14159265358
 GR = 8.31441

C RS: [mole/m^2s)]
C Total mass flow into surface: GFLX [kg/m^2s] Si

C Partial pressures in Pascals, Ea in kcal/mole, T in Kelvin

 P2=GPRESS*GX(2)
 P3=GPRESS*GX(3)
 Ea=36.73

C Rate is in mole/m^2s

 RS = A*exp(-Ea/(1.987E-3*GTEMP))*P2/
 1 (1 + Rh*SQRT(P3) + Rsi*P2)

 GFLX = -RS*MSI

C Store the convective flux
 GCON= -GFLX

C Calculate the deposition rate (nm/min) only if P1 is solved.
C [kg/m^2s] --> [nm/min]

 IF (GVAR .EQ. 1) GDEPO = RS*60.0*MSI*1.E9/RHOSI

C Correct the H2 flux: (a) compute the mass loss
C (b) adjust convection

 IF (GVAR .EQ. 3) GFLX = GMW(3)*RS*2
 IF (GVAR .EQ. 3) GFLX = GCON*GM(3)*2 + GFLX

C Correct the SiH4 flux: (a) compute the mass loss
C (b) adjust convection

 IF (GVAR .EQ. 2) GFLX = GMW(2)*RS
 IF (GVAR .EQ. 2) GFLX = GCON*GM(2) - GFLX
```

References

[1] J. I. Ulacia F., C. Werner, "Equipment Simulation: Part I," *Solid State Technology*, vol. 33, no. 11, pp. 107-113, 1990.

[2] Sherman, A., "Modeling of Chemical Vapor Deposition Reactors," *J. of Electronic Materials*, vol. 17, No. 5, 1988.

[3] K. K. Lin, "Modeling and Characterization of Semiconductor Manufacturing Equipment: An Application to LPCVD Reactors," *UC Berkeley Electronics Research Laboratory Memorandum No. UCB/ERL M90/44*, May 1990.

[4] S. Middleman, A. Yeckel, "A Model of the Effects of Diffusion and Convection on the Rate and Uniformity of Deposition in a CVD Reactor," *J. Electrochem. Society*, vol. 133, no. 9, pp. 1951-1956, 1986.

[5] K. F. Jensen, D. B. Graves, "Modeling and Analysis of Low Pressure CVD Reactors," *J. Electrochem. Society*, vol. 130, no. 9, pp. 1950-1957, 1983.

[6] K. F. Roenigk, K. F. Jensen, "Analysis of Multicomponent LPCVD Processes," *J. Electrochem. Society*, vol. 132, no. 2, pp. 448-454, 1985.

[7] W. A. P. Claassen et al., "The deposition of silicon from silane in a low-pressure hot-wall system," *J. Crystal Growth*, vol. 54, pp. 259-266, 1982.

[8] M. E. Coltrin, R. J. Kee, J. A. Miller, "A Mathematical Model of Silicon Chemical Vapor Deposition," *J. Electrochem. Society*, vol. 133, no. 6, pp. 1206-1213, 1986.

[9] E. Sachs, G. H. Prueger, R. Guerrieri, "An Equipment Model for Polysilicon LPCVD," *IEEE Transactions on Semiconductor Manufacturing*, vol. 5, no. 1, Feb. 1992.

[10] J. I. Ulacia F., C. Werner, "Equipment Simulation: Part II," *Solid State Technology*, vol. 33, no. 12, pp. 71-74, 1990.

[11] Creare Inc., Fluent Manual: Version 2.9, Hanover, New Hampshire 1987.

[12] D. B. Spalding, "The PHOENICS Beginner's Guide: CHAM TR/100," Cham Ltd., 1989.

[13] J. C. Ludwig, H. Q. Qin, D. B. Spalding, "The PHOENICS Reference Manual: CHAM TR/200," Cham Ltd., 1990.

[14] G. Fedder, "Physical Simulation of VLSI Process Equipment," U.C. Berkeley, *private communication*, 1991.

[15] C. J. Galewski, "Hot-Wall Silicon Epitaxy," *UC Berkeley Electronics Research Laboratory Memorandum No. UCB/ERL M90/122*, Dec. 1990.

[16] J. R. Welty, C. E. Wicks, R. E. Wilson, Fundamentals of Momentum, Heat, and Mass Transfer, 3rd ed., New York: John Wiley, 1984.

[17] R. B. Bird, W. E. Stewart, E. N. Lightfoot, Transport Phenomena, New York: Wiley, 1960.

[18] C. R. Wilke, "Diffusional Properties of Multicomponent Gases," *Chemical Eng. Progress*, vol. 46, no. 2, pp. 95-104, 1950.

[19] J. O. Hirschfelder, C. F. Curtiss, R. B. Bird, Molecular Theory of Gases and Liquids, New York: Wiley, pp. 1110-1112, 1954.

[20] C. R. Kleijn, H. H. van der Meer, C. J. Hoogendoorn, "A Mathematical Model for LPCVD in a Single Wafer Reactor," *J. Electrochem. Society*, vol. 136, no. 11, pp. 3423-3433, 1989.

[21] J. P. Jenkinson, R. Pollard, "Thermal Diffusion Effects in Chemical Vapor Deposition Reactors," *J. Electrochem. Society*, vol. 131, no. 12, pp. 2911-2917, 1984.

[22] M. E. Coltrin, R. J. Kee, J. A. Miller, "A Mathematical Model of the Coupled Fluid Mechanics and Chemical Kinetics in a Chemical Vapor Deposition Reactor," *J. Electrochem. Society*, vol. 131, pp. 425-434, 1984.

[23] W. A. Bryant, "The kinetics of the deposition of silicon by silane pyrolysis at low temperatures and atmospheric pressure," *Thin Solid Films*, vol. 60, pp. 19-25 1979.

[24] B. A. Murtagh, M. A. Saunders, "Modular In-core Nonlinear Optimization System (MINOS 5.3)," *Systems Optimization Laboratory, Dept. of Operations Research, Stanford University,* 1987.

[25] C. Hopfmann, J. I. Ulacia, C. Werner, Siemens research, *private communication,* 1991.

[26] B. S. Meyerson, J. M. Jasinski, "Phosphorous-doped polycrystalline silicon via LPCVD: Process characterization," *J. Electrochem. Soc.*, vol. 131, pp. 2361-2365, 1984.

[27] C. Werner, J. I. Ulacia F., S. Howell, "Numerical simulation of gas flow and chemical reactions in semiconductor processing equipment," *Symposium on VLSI Technology,* Kyoto, Japan, p. 49, May 1989.

[28] T. A. Badgwell, T. F. Edgar, et al, "Development of an Improved Fundamental Model for the Multiwafer LPCVD Reactor," *SRC Private Communication*, March 1991.

[29] C. Hopfmann, J. I. Ulacia, C. Werner, "Simulation of a Polysilicon LPCVD Reactor: Fluid -dynamics and Error Analysis," *private communication.*

[30] T. Kamins, Polycrystalline Silicon for Integrated Circuit Applications, Boston: Kluwer, 1988.